DESIGN OF EXPERIMENTS FOR HIGH-TEMPERATURE LITHIUM-ION BATTERY RESEARCH

A Thesis

Presented to

The Faculty of the Department of Mechanical Engineering

California State University, Los Angeles

In Partial Fulfillment

of the Requirements for the Degree

Master of Science

in

Materials Science and Engineering

By

David Allen Strickland

May 2024

© 2024

David Allen Strickland

ALL RIGHTS RESERVED

The thesis of David Allen Strickland is approved.

Chris Bachman, Committee Chair

David Raymond

Yixian Wang

Mohsen Eshraghi, Program Director

California State University, Los Angeles

May 2024

ABSTRACT

Design of Experiments for High-Temperature Lithium-Ion Battery Research

By

David Allen Strickland

NASA's Jet Propulsion Laboratory is currently developing the platform for a Venus-deployed aerobot mission that will operate in the planet's atmosphere at temperatures from -30°C to 100°C. Existing space-rated li-ion cells can be modified to operate at the lower temperature limit; however, operation at the higher temperature limit requires cell components, specifically the anode, cathode, and electrolyte, that resist degradation at high temperatures. Since the various components work in concert they must be tested simultaneously. Design of experiments is a framework suited for testing numerous factors at the same time. The purpose of this research is two-fold: to evaluate the viability of utilizing design of experiments (DOE) in lithium-ion battery research, and to improve the high-temperature performance of lithium-ion coin cells.

In this study, a 2^4 full factorial experiment was conducted after a preliminary ${2_{III}}^{5-2}$ fractional factorial experiment to quantitatively analyze and compare the main and interactive effects of a total of seven lithium-ion coin cell components on a total of six performance metrics between the two designs. The full factorial design tested every combination of factors and levels, while the fractional factorial design tested a selected quarter-fraction subset of possible trial combinations, in an approach that is more resource-efficient at the cost of aliasing effects. Completion of the study required the design of the experimental layout, cell assembly, solid electrolyte interphase formation, high-temperature charge/discharge cycling, experimental data analysis, and statistical analysis adapted for each of the two designs.

The results of the fractional factorial design verified the instability of lithium anodes at 100°C, showing a 75.0% fail rate versus 41.7% for cells with graphite anodes. The full factorial design showed that polyimide separators increased cycle life by 118.2%, increased total coulombic efficiency by 44.2%, and lowered end-of-discharge voltage post-rest by 4.8% compared to the tri-layer Tonen separators. The 1:1:1 NMC cathodes were found to increase cycle life by 39.3% compared to the 8:1:1 NMC cathodes. Synergistic interactions between the polyimide separators and 1:1:1 cathode were also found, including where the combination of the two increased cycle life by 187.9% over polyimide separators with 8:1:1 cathodes and 70.4% over 1:1:1 cathodes with Tonen separators. Other statistically significant interactions were also found and are detailed in the thesis.

This study demonstrates that DOE methodologies aid in the development and optimization of high-temperature lithium-ion batteries by having statistically identified the components with the greatest effect on cell performance and the synergistic interactions between them. The key findings of this work will lead to other experiments, helping further energy storage research with implications both in space and on Earth.

ACKNOWLEDGMENTS

I would like to express my deepest appreciation for the following individuals who have played pivotal roles in my academic journey and the completion of this study.

First and foremost, my advisor, Dr. Chris Bachman has been an inspiring mentor since my very first semester as an undergraduate at Cal State LA. Helping to instill in me the importance of curiosity, independent learning, and critical thinking, his guidance, encouragement, and passion for research have shaped not only my academic path, but my aspirations for the future.

This thesis is the result of the diligent work and thoughtful planning contributed by myriad people at both Cal State LA and JPL. I would like to personally acknowledge:

Dr. Will West at JPL, without whose direction and expertise this work would not have been possible. His willingness to be directly involved, listen to my ideas, and try different solutions was crucial to the success of this research.

Jasmina Pasalic, whose help with cell building, equipment setup, and testing at JPL was invaluable.

My thesis committee: Dr. David Raymond and Dr. Yixian Wang, whose patience, feedback, and foundational lessons in their respective fields provided the groundwork for this study.

Dr. Mohsen Eshraghi, Director of the Materials Science and Engineering Program, for recognizing and promoting the value of interdisciplinary fields.

At the periphery of this thesis are all the professors, administrators, students, and organizations that have, for years, been sources of knowledge, assistance, motivation, and camaraderie.

While all professors deserve recognition, a special mention goes to Dr. Brieu, Dr. Santner, Dr. Sharif, Dr. Medina, and Prof. Henandez. Their teachings during my time in the B.S. ME program equipped me with the fundamental knowledge necessary for the advanced research I aspire to purse in my career.

Mayra Alonzo, at the Department of Mechanical Engineering for always being quick with an answer and a point in the right direction.

Dr. Pacheco-Vega and everyone at CATSUS for providing the support and exposure to new and exciting research topics, especially those that highlight sustainability through engineering.

All my fellow researchers at the Sustainable Technology Lab at CSULA through the years but especially: Arnoldo Rendon, Jose Rochin, Juan Lima-Rietos, Wit Udomnopwitthayakul, Henry Amador, and Alan Rodriguez.

My family, for always believing in me. Love you, Mom and Amanda.

And finally, if I've learned anything in the last four or five degrees, it is that no one can truly go it alone, and I've been lucky enough not to have to. Thank you to Nicole, my wonderful, beautiful partner, who has been my rock, my compass, and my wings.

TABLE OF CONTENTS

Abstract iv

Acknowledgments vi

List of Tables x

List of Figures xi

Chapter

1. Introduction 1

1.1 Motivation for High Temperature Lithium-Ion Batteries and Design of Experiments 1

1.1.1 JPL Mission to Venus 1

1.1.1.1 Mission Description 2

1.1.1.2 Power Requirements 3

1.1.2 Lithium-Ion Batteries 3

1.1.2.1 Basic Operating Principles and Key Components 4

1.1.2.2 Limitations and Behavior at High Temperature 8

1.1.2.3 DOE and its use in LIB studies 10

2. Methodology 13

2.1 Experiment Design 13

2.1.1 Fractional Factorial Experiment 13

2.1.2 Full Factorial Experiment 14

2.2 Li-ion Coin Cell Assembly 15

2.3 Cell Cycling 16

2.4 Experimental Data Analysis 17

3. Results and Discussion 19
3.1 Fractional Factorial Experiment 19
3.1.1 Experimental Results 20
3.1.1.1 Cycle Life 22
3.1.1.2 Average Coulombic Efficiency 24
3.1.1.3 Cell Lifetime 25
3.1.2 Discussion 28
3.2 Full Factorial Experiment 31
3.2.1 Experimental Results 32
3.2.1.1 Pass/Fail 33
3.2.1.2 Cycle Life 35
3.2.1.3 Total Coulombic Efficiency 39
3.2.1.4 End-of-Discharge Voltage Post-Rest 41
3.2.2 Discussion 44
4. Conclusions 48
4.1 Summary 48
4.2 Conclusion 48
4.3 Future Work 50
References 51
Appendix
Experimental Layouts 54

LIST OF TABLES

Table

1. Factors and Levels for Fractional Factorial Design 14
2. Factors and Levels for Full Factorial Design 15
3. Step Details for Battery Cycling 17
4. Response Values for Fractional Factorial Experiment 20
5. Response Values for Full Factorial Experiment 33
6. Experimental Layout for Fractional Factorial Design 54
7. Experimental Layout for Fractional Factorial Design 55

LIST OF FIGURES

Figure

1. JPL Venus Aerobot 2
2. Energy Densities of Various Secondary Cell Chemistries 4
3. Exploded View of CR2032 Coin Cell 5
4. Schematic of Li-ion Cell Basic Operation 8
5. DOE Study Areas.....11
6. Cube Plots of Full and Fractional Factorial Designs 11
7. Cell Assembly and Finished Block of Cells 16
8. Experiment 1 Cycle Life Normal Probability Plot 22
9. Experiment 1 Cycle Life Pareto Chart.....23
10. Experiment 1 Cycle Life Main Effect Plot 23
11. Experiment 1 Average Coulombic Efficiency Normal Probability Plot 24
12. Experiment 1 Average Coulombic Efficiency Pareto Chart.....25
13. Experiment 1 Cell Lifetime Histogram.....26
14. Experiment 1 Cell Lifetime Normal Probability Plot.....26
15. Experiment 1 Cell Lifetime Pareto Chart 27
16. Experiment 1 Cell Lifetime Main Effect Plot.....28
17. Experiment 1 Pass/Fail Normal Probability Plot.....29
18. Experiment 1 Pass/Fail Pareto Chart 30
19. Experiment 1 Pass/Fail Main Effects Plot 30
20. Cell 2-40 Voltage vs Elapsed Time 34
21. Experiment 2 Pass/Fail Normal Probability Plot.....35

22. Experiment 2 Cycle Life Normal Probability Plot 36

23. Experiment 2 Cycle Life Pareto Chart.....37

24. Experiment 2 Cycle Life Main Effects Plot.....38

25. Experiment 2 Cycle Life Interactive Effects Plot.....39

26. Experiment 2 Total Coulombic Efficiency Normal Probability Plot.....39

27. Experiment 2 Total Coulombic Efficiency Pareto Chart.....40

28. Experiment 2 Total Coulombic Efficiency Main Effect Plot 41

29. Experiment 2 End-of-Discharge Voltage Post-Rest Normal Probability Plot.....41

30. Experiment 2 End-of-Discharge Voltage Post-Rest Pareto Chart.....42

31. Experiment 2 End-of-Discharge Voltage Post-Rest Main Effect Plot 43

32. Experiment 2 End-of-Discharge Voltage Post-Rest Interactive Effects Plot.....44

CHAPTER 1

Introduction

1.1 Motivation for High Temperature Lithium-Ion Batteries and Design of Experiments

NASA's Jet Propulsion Laboratory seeks to develop battery cells that will enable missions that will experience a temperature range of -30° C to 100° C. Current space-rated li-ion cells can be tailored to meet the lower temperature limit, however, operating or storage temperatures of roughly 60° C and higher can rapidly degrade cell performance. Thus, a new mission-enabling battery cell technology must be developed that can tolerate such temperature extremes [1].

In addition to its astronautical implications, improved energy storage technology would have applications here on Earth. The increasing demand for high performance, fast-charging batteries in electric vehicles and personal electronics, particularly in hot climates like those experienced by urban populations around the equator, can be met with the development of cells that can perform at a higher operating temperature threshold.

1.1.1 JPL Mission to Venus

For over twenty years, JPL has planned a return to Venus [2]. Often called Earth's sister planet, Venus is similar in size, mass, composition, and distance from the sun. It is possible that billions of years ago, Venus had liquid water on its surface and an atmosphere like Earth's, but volcanic activity led to a runaway greenhouse gas effect that drastically changed the planet's atmosphere. Previous exploration has revealed a dense atmosphere of carbon dioxide and clouds of sulfuric acid, with surface temperatures of up to 460° C and an atmospheric pressure over ninety times that of Earth [3]. Continuing to

study Venus may provide clues on how Earth-like planets can change over time. To that end, JPL's latest efforts in research and development of an exploratory mission to Venus center on a balloon-based robotic vehicle called an aerobot.

1.1.1.1 Mission Description

The Venus Aerobot concept is a variable-altitude research platform designed to be deployed for approximately one hundred days of cloud-level exploration just below the transition zone between the troposphere and mesosphere of Venus at an altitude range of 52 to 62 km. An artist's rendition of the Venus Aerobot is shown in Figure1.



Figure 1. JPL Venus Aerobot. Illustration of Venus Aerobot hanging from a variable buoyancy balloon in the Venusian atmosphere [4].

With a mission focus of atmospheric circulation, seismography, and remanent magnetism, the aerobot will float east to west circumnavigating the planet once about

every six days. The variable-buoyancy design is a balloon-within-a-balloon system that uses a pump to store helium in the inner, super pressure balloon for descent, and vents to release the stored helium into the outer, zero-pressure balloon for ascent. This setup will carry a mass of 100 kg that includes all subsystems: structure, flight computer, scientific instruments, telecommunication, thermal management, and power systems and is scalable to allow for mission flexibility [4].

1.1.1.2 Power Requirements

One of the main focuses for the design is to have power generation and energy storage that is sufficient for the onboard systems. While on the daytime side of Venus, an acid-resistant solar array is expected to generate 200-300 W for high-draw applications like telecommunications events and helium pumping for reduced-buoyancy descent as well as charging batteries for nighttime operation [5]. To coincide with the mission design, these batteries must be lightweight, power-dense, and able to be stored and operate at the temperatures in target altitude of the Venusian atmosphere – between -30° C and 100° C.

1.1.2 Lithium-Ion Batteries

Lithium-ion batteries (LIBs) are currently one of the most advanced rechargeable battery chemistries available [6]. Compared to their nickel-based predecessors, LIBs offer higher gravimetric and volumetric energies as shown in Figure 2. Additionally, they provide higher single cell voltage, and do not suffer from a memory effect. Importantly

they also come in various form factors, which improves packaging of the energy storage within the system.

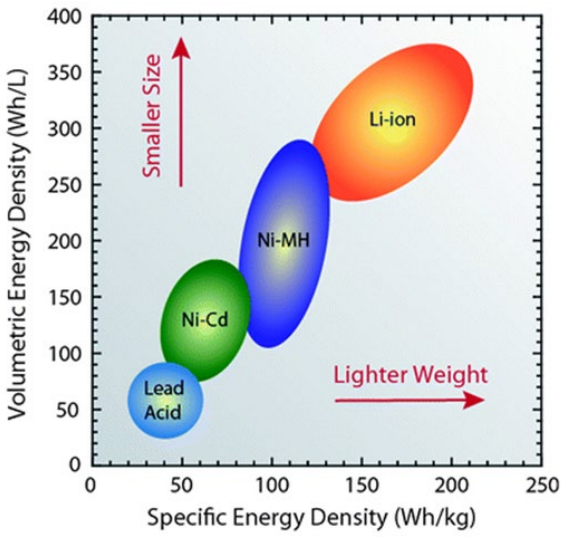


Figure 2. Energy Densities of Various Secondary Cell Chemistries. Li-ion batteries have both higher specific and volumetric energy densities than nickel or lead-based secondary battery chemistries [7].

1.1.2.1 Basic Operating Principles and Key Components

A LIB is made up of multiple individual li-ion cells that can be wired in series for increased voltage, parallel for increased current, and in combined configurations to match required power specifications. Each cell consists of the following basic components in this order: a positive electrode (cathode), a separator, and a negative electrode (anode); with all three components wetted by an electrolyte. Other components like current collectors, spacers, wave springs, and containers are present and can be design-specific. A diagram of a CR2032 coin cell is shown in Figure 3.

The cathode material is critical to the performance of LIBs and in some cases the cathode itself can account for up to 40% of the cost of the battery [8]. Material selection

should consider the following property/characteristic relationships: a high working potential will increase the positive limit of the cell potential; high lithium ion and electron conductivities lead to high power density; the ability to accommodate a large amount of lithium increases specific capacity; and good reversibility of lithium ion insertion and extraction with minimal volume change can help increase cycle life [9]. The most used cathode materials are layered transition metal oxides (e.g.: $LiCO_2$, $LiNiO_2$, $LiMnO_2$) that serve as intercalation hosts for the lithium ions, creating a continuous solid solution when the cell is discharged. Cells are often fabricated in the discharged state as the discharged cathode and anode materials are stable in atmosphere.

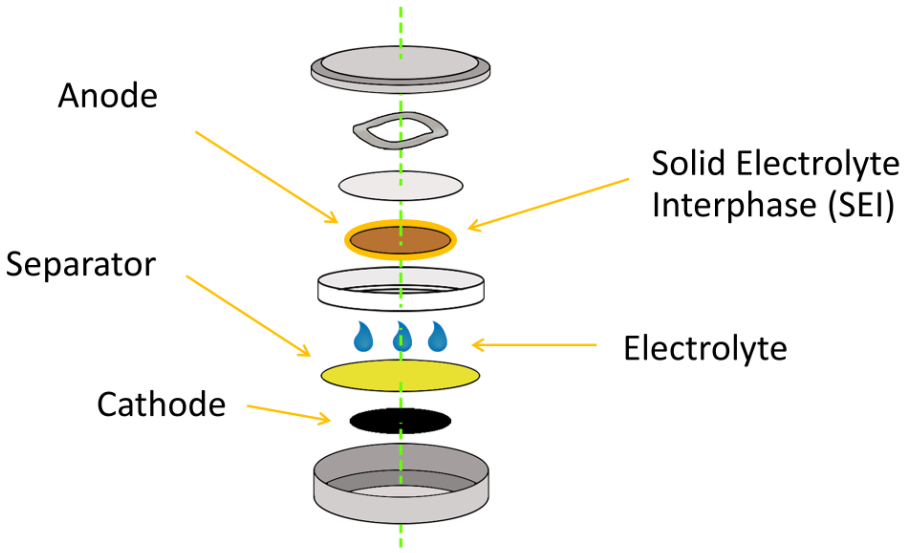


Figure 3. Exploded view of CR2032 coin cell.

The separator serves the crucial task of preventing short circuits in cells that utilize liquid electrolytes by ensuring that the positive and negative electrodes do not make direct contact. The following properties are typically required for a proper separator: good chemical stability and inertness in contact with other cell components,

mechanical durability such as to endure tension and resist puncture by electrode materials, and a pore size of less than 1μm. Polymer membranes offer these properties as well as other desirable traits including permeability, wettability, dimensional stability, and cost. Multilayer polymer composites can also be made as a form of thermal fuse, preventing combustion caused by thermal runaway [6].

A suitable anode is another key component of high-energy LIBs. The first LIBs used lithium metal anodes as they offered a high specific capacity. It was found however that the non-uniform replating of li-ions during charging promotes dendrite growth through the separator which could cause the cell to short circuit and explode. Graphite has since become the most widely used material due to its overall performance. As with the cathode, the anode material should be chosen with consideration of its conductivities and capacity to accept intercalated lithium ions. In addition, the anode should have a low redox potential to pair with the higher potential of the cathode for an increased cell potential and it should allow for the formation of a dense and stable solid electrolyte interphase (SEI).

The SEI is a film that forms around the anode during the first charging cycle. The low potential at the negative electrode surface induces decomposition of the immediately surrounding electrolyte isolating the anode surface from the electrolyte and avoiding further decomposition during subsequent cycles. If the SEI is poorly formed, continued electrolyte decomposition can increase the thickness of the SEI, potentially causing a higher internal resistance and lower lithium insertion reversibility, resulting in decreases in energy density as the cell is cycled. Chemical composition of the SEI can be characterized, and it is generally believed to be ionically conducting and electrically

insulating like the parent electrolyte, however, the actual formation mechanism is poorly understood [6].

Lastly, the liquid electrolyte is the key component that serves as a continuous medium of transport for the lithium ions from one electrode, through the separator, and to the opposite electrode. The electrolyte must be an ion conductor and electrical insulator, it must be stable at the appropriate cell potential range, and it must remain liquid at all operating temperatures [8]. The typical electrolyte in LIBs is a solution of organic solvents and lithium salts. Aprotic carbonates like ethyl carbonate and dimethyl carbonate can be mixed to increase their liquidus range, are stable at the potential range of LIBs, and when decomposed, provide material for the SEI. Additionally, their high dielectric constant helps dissolve high concentrations (e.g.: 1M) of lithium salts like $LiPF_6$ and $LiBr_4$.

A schematic showing the operation of a li-ion cell is shown in Figure 4. When the cell is charged, an external power supply connected to current collectors on both electrodes causes a release of electrons from the cathode material and allows them to flow through the external circuit to the anode. To maintain charge balance, the oxidized Li ions also migrate from the intercalated sites in the cathode, diffusing internally through the separator pores via the electrolyte, then through the SEI to an intercalated site in the anode. This stores the external energy from the power supply in the form of chemical energy in the anode material. When the stored energy in the cell is required to do work, the cell is discharged. Here, the external power supply is replaced by an external load and the opposite process occurs, whereby the electrons and Li ions take their respective paths from the anode to the cathode. The rate at which this process occurs is quantified by the

current or a normalized form of the current known as C-rate. C-rate is defined as the charging or discharging current divided by the capacity of the battery [10].

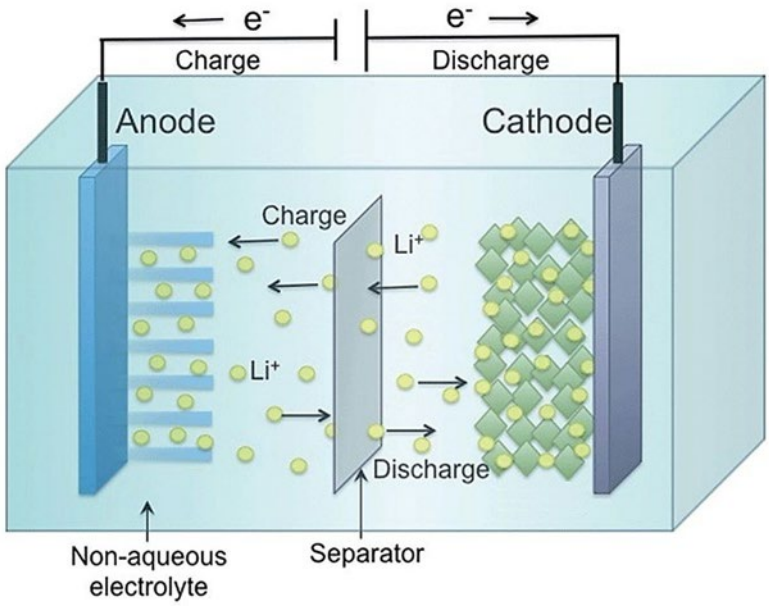


Figure 4. Schematic of Li-ion Cell Basic Operation [11].

1.1.2.2 Limitations and Behavior at High Temperature

In general, LIBs exhibit best-in-class working performance so long as they are operated within the acceptable temperature region of -20° C to 60° C, with an optimal range of 15° C to 35° C [12]. Operation at temperatures near and above the upper threshold results in battery degradation, accelerated aging, and can result in thermal runaway, leading to serious safety risks [13].

Battery degradation and aging include various mechanisms that cause the loss of both cell capacity and power because of their impact on the thermodynamic and kinetic behavior of the cell [14]. These impacts include the losses of cathode material, lithium inventory, and electrolyte, as well as changes in crystal and chemical structure.

In cathodes with layered Ni-rich oxides, several degradation mechanisms have been studied including Li^+/Ni^{2+}cation mixing, oxygen evolution, transition metal dissolution, and particle cracking [15]. A high state of charge and high temperature can cause Li^+/Ni^{2+}cation mixing (where the similar cation size can result in Ni^{2+} migrating to interstitial Li^+ sites) and oxygen evolution, resulting in low-valence metal oxide-formation. Concurrently, gas evolution of CO_2 and CO in the electrolyte are accompanied by the formation of H_2O which hydrolyzes the commonly used lithium salt solute $LiPF_6$ in the electrolyte. This hydrolysis produces HF which reacts with the low-valence metal oxides, collapsing the cathode surface structure and resulting in capacity decay.

At the anode, one mechanism for degradation is the intercalation of solvent in the carbon layers. This can cause the exfoliation of carbon and subsequently, the expansion of carbon particles, forming graphite intercalation compounds leading to the loss of active material and contributing to irreversible capacity loss [16]. This effect is enhanced at higher operating temperatures, however, the degradation of the anode's effectiveness in providing its stored lithium ions is mainly attributable to the SEI layer around the anode [17].

Although the SEI is formed during the first charging cycle, its thickness increases as the cell ages, correlating with the square root of time. At elevated temperatures, diffusion and side reaction rates increase, which increases the SEI growth rate. As the SEI grows, it can trap lithium ions, lowering the inventory of charge carriers and thereby reducing cell capacity. Additionally, it can block separator pores, consume electrolyte solvent, and become increasingly difficult for lithium ions to penetrate, all of which increase cell impedance and result in power loss [14].

1.2.3 DOE and its use in LIB studies

Though DOE is well known in academia and industry and has seen a long history of success in industries like pharmaceuticals, agriculture, energy, and analytical chemistry, only within the last ten years has it started to see more widespread use in the field of lithium batteries [18]. Hence, a brief discussion is warranted as the use of DOE to examine its viability for use at JPL falls within the objective of this study.

DOE is a branch of statistics used to design, plan, and analyze an experiment to explore the individual and interactive effects of multiple quantitative or qualitative factors on a defined output, ensuring valid and objective engineering conclusions are attained [19]. It is based on the principles of randomization, blocking, replication, factorial approach, and analysis of variance. As shown in Figure 5, it is a versatile technique that is used in the following study areas: comparative, screening, modeling, optimization, robust design, and formulation.

The 2^k Factorial Design is appropriate for the preliminary stages of experimental work where many factors are being considered. Where k is the number of factors to be studied, 2^k provides the smallest number of trial runs for one complete replicate of a Full Factorial Design, i.e., every combination of each factor at each level. A Fractional Factorial Design (2_i^{k-n}) tests a $\frac{1}{2^n}$ fraction of the Full Factorial Design where the subscript denotes design resolution, or the extent of aliasing present as illustrated in Figure 6.

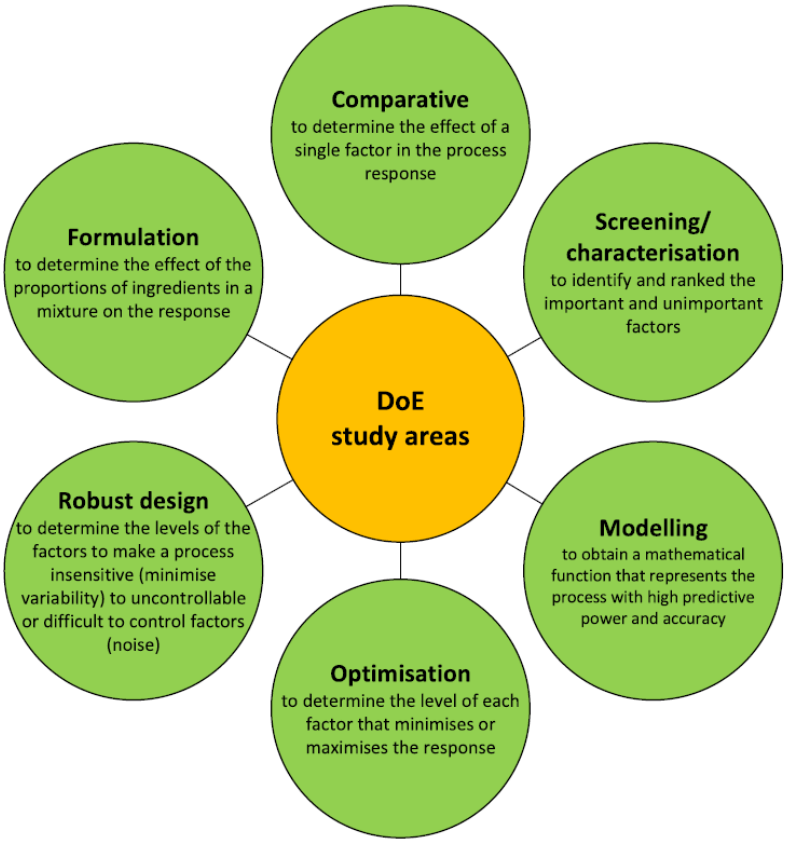


Figure 5. DOE Study Areas. Design of experiments is well suited for various study areas including comparative studies, screening/characterization, modelling, optimization, robust design, and formulation [18].

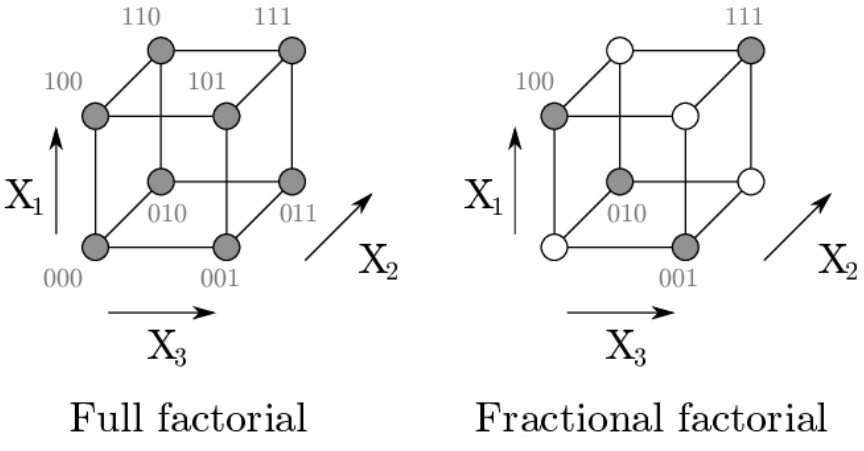


Figure 6. Cube Plots of Full and Fractional Factorial Designs. For a 2^3 factorial design, all eight combinations of factors at their different levels are represented. In a 2^{3-1} fractional factorial design tests half of the possible combinations at the cost of aliasing [20].

These types of designs are advantageous for conserving time and resources and are useful in factor screening experiments. In both designs, the assumption is made that the response is linear between quantifiable values since each factor in this design has only two levels [20]. For qualitative factors, this assumption is not necessary. Main effects are regarded as a difference in the response value at each level of a given factor. Interactions are when the effect of one factor depends on the level of another factor [19]. The null hypothesis for the statistical analysis of the results is that no factor or combination of factors will have an effect on the response variable.

A very brief overview of the methodology follows: a problem and the study objectives are stated; the factors and their appropriate levels, as well as the response(s), are chosen; an experimental design is chosen; the experiment is performed according to the design; the data is collected and analyzed using ANOVA, graphical methods (e.g.: Pareto charts, histograms, and mean plots), and empirical models; the results provide a basis for an objective conclusion. Specific designs, methodologies, and equations are available in various texts and publications [19] [20] [21] [22].

CHAPTER 2

Methodology

This study required an extensive preparatory phase dedicated to understanding the fundamentals and application of DOE, as well as the operating principles of li-ion cells as relevant in high-quality cell assembly and cycling, and extensive use of analytical software. The following sections detail the methodologies for each phase of the study.

2.1 Experiment Design

For both experiments in this study, factorial designs were used to test the independent variables (factors) at two quantitative values or qualitative types (levels). Each experiment was designed with three replicates to account for variability and in three blocks to account for uncontrollable factors like room temperature that could affect the results. Each block consisted of one replicate where all the replicate's cells were fabricated and started on SEI formation cycling on the same day.

Minitab was used to design the experimental layout for each experiment, which provided the randomized run order within each replicate. In this study, the run order was taken as the build order since all cells in each replicate would be tested simultaneously.

2.1.1 Fractional Factorial Experiment

A 2_{III}^{5-2} Fractional Factorial Design was directed for the initial experiment. In this case, the thirty-two total trial combinations of the five factors were reduced to eight per replicate. As a Resolution III design, main effects are aliased with two factor interactions and some two factor interactions could be aliased with others. The

assigned factors in this experiment were the following: SEI Formation C-Rate at levels of C/20 vs 1 C, Charge/Discharge C-Rate at levels of C/20 vs 1 C, Phosphorodifluoridate (electrolyte additive) at levels of Added vs Omitted, Anode material at levels of Lithium vs Graphite, and Vinyl Carbonate (electrolyte additive) at levels of Added vs Omitted. Experimental variables were assigned to each factor according to the aliasing combinations that were expected to conserve the interactive effect between the two electrolyte additives. Table 1 shows the high and low levels for each factor as well as the experimental variable assigned to each for use during design and analysis.

Table 1. Factors and Levels for Fractional Factorial Design.

Factor	**Name**	**Low (-1)**	**High (1)**
A	SEI	C/20	1C
B	Ch/Disch	C/20	1C
C	PDF	Added	Omitted
D	Anode	Lithium	Graphite
E	VC	Added	Omitted

An experimental layout was generated in Minitab and is shown in Table A-1 in the Appendix. The cells were numbered according to their order in each block and the blocks were scheduled sequentially.

2.1.2 Full Factorial Experiment

A 2^4 Full Factorial Design was used for the second experiment. Here, all sixteen trial combinations of the four factors at their low and high levels were tested. The assigned factors were: Phosphorodifluoridate at levels of Omitted vs Added, Vinyl Carbonate at levels of Omitted vs Added, cathode material at levels of an NMC oxide with a 1:1:1 ratio vs 8:1:1 ratio, and separator material of levels Tonen vs Polyimide.

Table 2 shows the high and low levels for each factor as well as the experimental variable assigned to each for use during design and analysis.

Table 2. Factors and Levels for Full Factorial Design.

Factor	Name	Low (-1)	High (1)
A	PDF	Omitted	Added
B	VC	Omitted	Added
C	Cathode	1:1:1	8:1:1
D	Separator	Tonen	Polyimide

An experimental layout was generated in Minitab and is shown in Table A-2 in the Appendix. The cells were numbered according to their order in each block and the blocks were scheduled by run order.

2.2 Li-ion Coin Cell Assembly

A total of seventy-two li-ion cells were assembled at JPL across both experiments. The cells for the initial experiment were assembled in an argon glove box while those for the second were assembled in a dry room with a water vapor concentration of 150 ppm. The initial assembly process consisted of stacking components in the following order: the positive half of a stainless steel CR2032 coin cell case, a 1.98 cm^2 lithium NMC cathode of either 1:1 or 8:1:1 ratio with an aluminum current collector, a separator of either tri-layer Tonen or polyimide, an O-ring, 100 µL of an electrolyte solution of $LiPF_6$ salt and EC:EMC in a 1:1 ratio with either 2% wt. EC, 2% wt. PDF, both, or neither, an anode of lithium metal or graphite with a copper current collector, a 1mm stainless steel spacer, a stainless steel wave spring, and the negative side of the coin cell case. The trial combinations listed in the two experimental layouts shown in Tables A-1 & A-2 indicate

which of the anode, separator, electrolyte, and cathode were used. After the components were stacked, the assembly was crimped shut. Tabs to clip test leads on to were welded to each side then epoxy was used to seal the cell along the crimp seam. Figure 7 shows the assembly setup in the dry room at JPL as well as the completed set in Block 2 of the full factorial experiment.

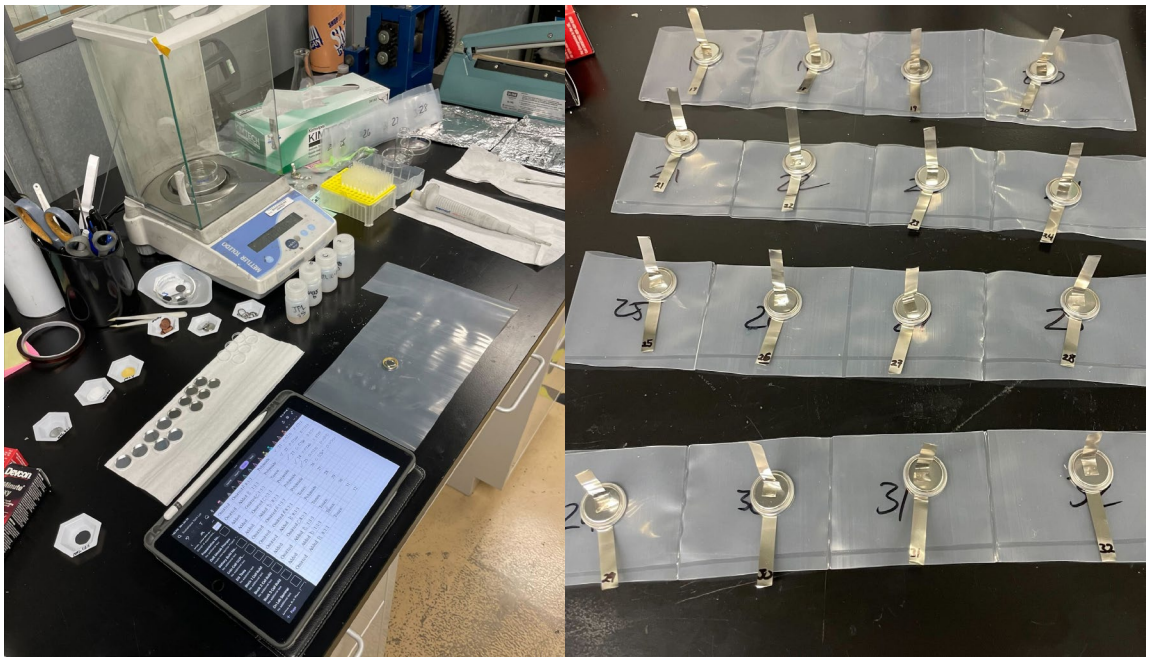


Figure 7. Cell Assembly and Finished Block of Cells. Cells for the full factorial experiment being assembled in a dry room at JPL (left). A completed block of 16 cells representing all trial combinations in the 2^4 factorial experiment (right).

2.3 Cell Cycling

The cells in the fractional factorial experiment were cycled on an Arbin battery cycling system. The SEI formation was done at room temperature and consisted of 5 cycles at C-rates of either C/20 or 1C depending on the trial combination for each cell. These rates were based on a theoretical cell capacity of 3.7 mAh. After the SEI formation cycling, the cells were cycled in a Blue M Stable Therm Gravity Oven at 100° C, and

again at C-rates of either C/20 or 1C for a maximum of fifty cycles. Table 3 shows the schedule followed by the Arbin system.

Table 3. Step Details for Battery Cycling.

Step	Task	Limit Value
1	Constant Current Charge	4.2 V
2	Constant Voltage Hold	1 hour
3	Rest	15 minutes
4	Constant Current Discharge	2.5 V
5	Rest	15 Minutes

The cells in the full factorial experiment were cycled on a Maccor battery cycling system. The SEI formation was done at room temperature and consisted of 5 cycles at a C/20 C-rate. These rates were also based on a theoretical cell capacity of 3.7 mAh. After the SEI formation cycling, the cells were cycled in a Tenny Environmental Test Chamber at 100° C, at a C-rate of C/5 for a maximum of fifty cycles. The step schedule followed by the Maccor system was the same as the fractional factorial experiment. In both experiments, if the cell failed to reach 4.2 V during the charging cycle or 2.5 V during the discharge cycle in less than 48 hours, the system would end the test.

2.4 Experimental Data Analysis

In both experiments, data was exported and collected from the Arbin or Maccor system, only after all cells of the given block had completed testing in each phase – SEI formation and 100° C cycling. MATLAB scripts were developed to process the raw data and compute the desired response variables for each experiment. The responses were then entered into their respective Minitab projects to analyze the MATLAB-derived results

according to their factorial design. The results for each experiment are presented and discussed separately in Chapter 3.

CHAPTER 3

Results and Discussion

At its inception, this study was a way of discovering any potential interaction between the two electrolyte additives of interest developed at JPL. However, the opportunity was taken to include various other factors to evaluate not only their potential effects but also to test the robustness and reliability of a fractional factorial design as compared to a full factorial design. This chapter presents the results of extensive analysis of the data collected from each design as well as discussions on what was learned and some subsequent decisions for continuing with the study.

3.1 Fractional Factorial Experiment

In the 2_{III}^{5-2} fractional factorial design, the responses were cycle life, cell lifetime, and coulombic efficiency. For this study, cycle life was defined as the whole number of cycles before the discharge capacity of the battery reached 40% of its initial capacity. The initial capacity was defined as the discharge capacity of the cell after the initial charge/discharge cycle at 100° C. The last cycle to meet this criterion is also referred to as the last live cycle. The cell lifetime is the total elapsed time from the beginning of the cycling process at 100° C until the end of the last live cycle. The coulombic efficiency was taken as the average of the coulombic efficiencies of the last three live cycles and was calculated using the recorded charge and discharge capacities as shown in Equation 1.

$$CE = \frac{1}{n}\sum_{i=1}^{n}\frac{discharge\ capacity_i}{charge\ capacity_i} \qquad \text{Eq. 1}$$

In most cases $n = 3$, however in the cases where the cell did not complete three cycles, the average was taken from the last 2 cycles or was taken as the value of the first and only cycle.

3.1.1 Experimental Results

A MATLAB script was developed for organizing, tabulating, and plotting relevant information. Table 4 shows the responses for each of the twenty-four cells.

Table 4. Response Values for Fractional Factorial Experiment.

Cell #	Cycle Life	Cell Lifetime [h]	Avg CE	Avg CE (Imputed)
1-1	6	230	73%	73%
1-2	3	4.4	91%	91%
1-3	2	1.0	0.00%	0.00%
1-4	4	2.0	180000000%	53%
1-5	1	0.97	31%	31%
1-6	12	160	250%	31%
1-7	5	12	74%	74%
1-8	4	82	110%	75%
1-9	29	46	99%	99%
1-10	1	1.2	0.13%	0.13%
1-11	1	190	0.06%	0.06%
1-12	1	43	37%	37%
1-13	14	11	91%	91%
1-14	2	80	31%	31%
1-15	12	170	75%	75%
1-16	3	5.3	86%	86%
1-17	50	69	101%	101%
1-18	12	27	98%	98%
1-19	3	100	102%	102%
1-20	4	120	74%	74%
1-21	1	0.50	0.02%	0.02%
1-22	1	0.50	1000%	31%
1-23	50	110	105%	105%
1-24	50	90	96%	96%

It is noted that the average coulombic efficiency values for cells 1-4, 1-6, 1-8, and 1-22 are well outside the acceptable values for coulombic efficiency. The inclusion of

these values skews the mean, standard deviation, and range of the data, reducing the power of statistical tests. While the standard response to this situation would be to omit the problematic data, in a blocked DOE study, the result would be unbalanced design [22]. Instead, a tactic known as mean imputation [23] was employed to replace these values and allow for preliminary analysis. With this method, the mean of the cell replicates was used as a substitute for the values of coulombic efficiency that were out of the possible range. The response data was then added to the experimental layout in Minitab to analyze the factorial design. A confidence level of 95% was selected. Minitab runs a linear regression to develop a model with a best fit line, whose R^2 value is given as a measure of the accuracy of the model. Residuals for each trial response are measured against the model and a normal probability plot is given showing the linear model as a red line. The "fat pencil test' is used as an informal approximation to verify the normality of the residuals and therefore that of the sample data [24].

In this section, the results for each of the three response variables are presented in a sequential manner. First, the normal probability plot for the given response is given to validate the use of the subsequential statistical methods. The Pareto chart then shows the absolute value of the standardized effect, or t-score, compared to the critical t-value, where any factor that crosses the critical t-value threshold is considered to have a statistically significant effect on the response with a P-value of less than the confidence level of $\alpha = 0.05$. Factorial means plots are then given to show the main effect or interaction for any model term with a statistically significant change in the response to show the effect of each term's level on the response mean at that level. Lastly, employing the Sparsity of Effects Principle, which states that most systems are dominated by main

or second-order interactions [22], data analysis through Minitab only included interactive terms of up to two factors in the regression model.

3.1.1.1 Cycle Life

In Figure 8, the normal probability plot for Cycle Life shows that the response residuals align acceptably well with the expected behavior assumed under a normal distribution. The model summary reported an R^2 value of 53.03%.

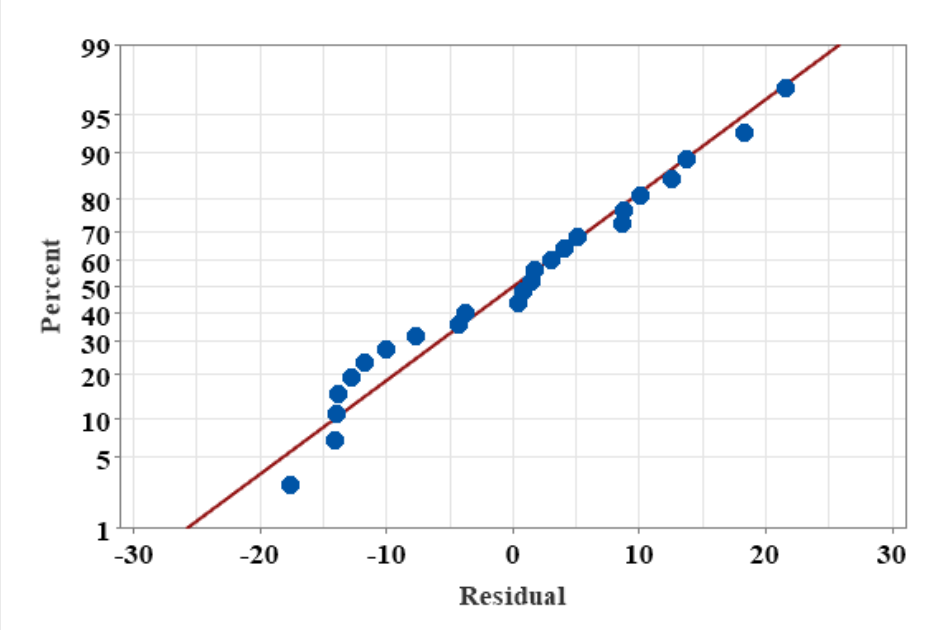


Figure 8. Experiment 1 Cycle Life Normal Probability Plot.

The Pareto chart in Figure 9 shows the absolute value of the critical t-score of 2.145 and that the charge/discharge C-rate is the only statistically significant factor with a standardized effect of 2.39.

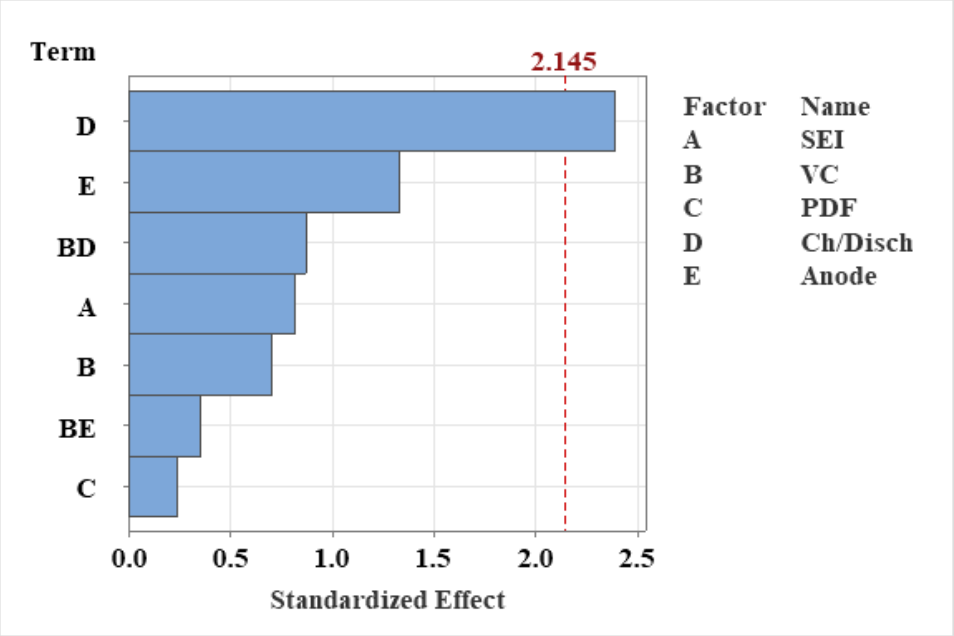


Figure 9. Experiment 1 Cycle Life Pareto Chart.

The means plot for the main effect of the charge/discharge c-rate is shown in Figure 10. Here, we see that the mean of cycles with a discharge capacity of at least 40% the initial discharge capacity at 100° C goes from 4.33 cycles at C/20 to 18.25 cycles at 1C.

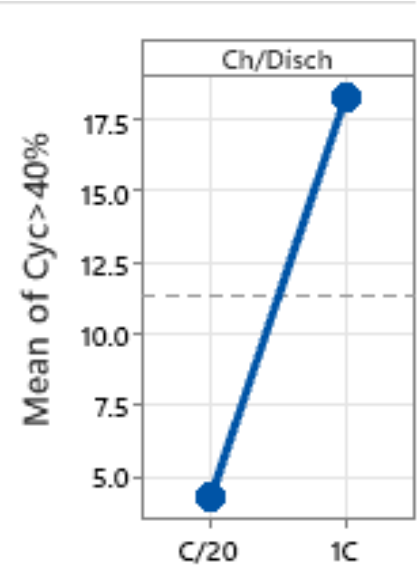


Figure 10. Experiment 1 Cycle Life Main Effect Plot.

3.1.1.2 Average Coulombic Efficiency

Although efficiency values should never exceed 100%, values between 100% and 110% were used in the analysis as it can be reasonably assumed that these values are the result of unanticipated electrochemical side-reactions.

In Figure 11, the normal probability plot for average coulombic efficiency shows that the assumption of normally distributed data is valid. The model summary reported an R^2 value of 46.59%.

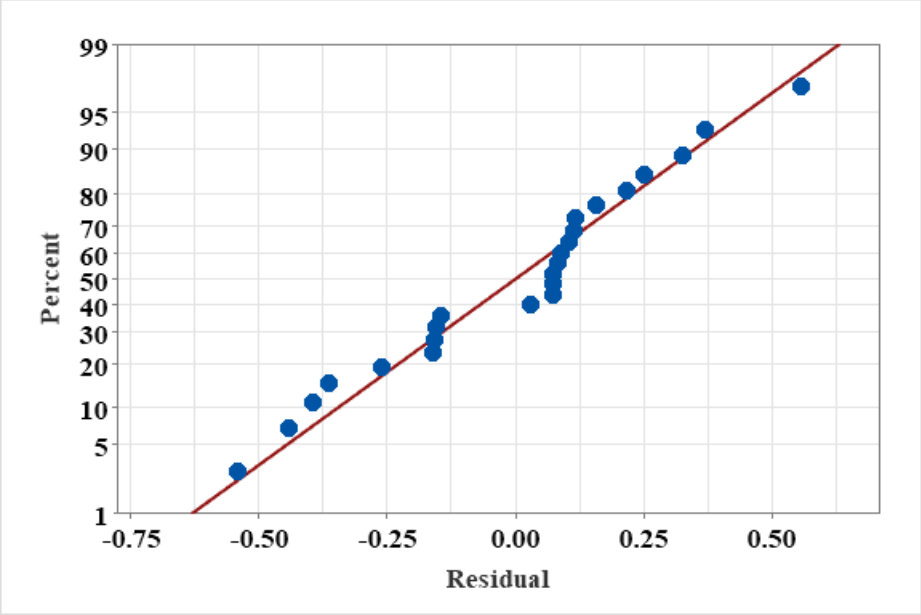


Figure 11. Experiment 1 Average Coulombic Efficiency Normal Probability Plot.

The Pareto chart in Figure 12 shows the absolute value of the critical t-score at 2.145 and that no model term had a standardized effect that crossed that threshold; therefore, no factor or combination of factors showed a statistically significant effect on the average coulombic efficiency response.

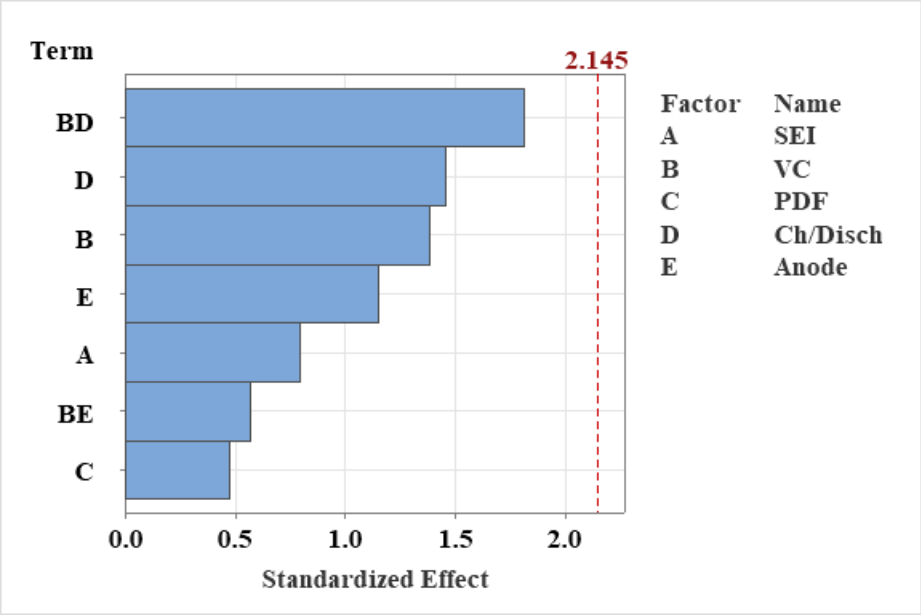


Figure 12. Experiment 1 Average Coulombic Efficiency Pareto Chart.

3.1.1.3 Cell Lifetime

Cell lifetime is taken as the elapsed time, measured from the start of the first charging cycle to the end of the last live cycle. The histogram plot shown in Figure 13 was made to look for a general trend in how long the cells lasted at 100°C. It was found that ten of the twenty-four cells failed within the first 24 hours, but there was not a specific amount of time that cells typically lasted.

Figure 14 shows that the normal probability plot for cell lifetime is not as linear as the other responses, however, by employing the "fat pencil test," it is adequate to assert that the assumption of normality for this study is valid. The model summary reported an R^2 value of 40.76%.

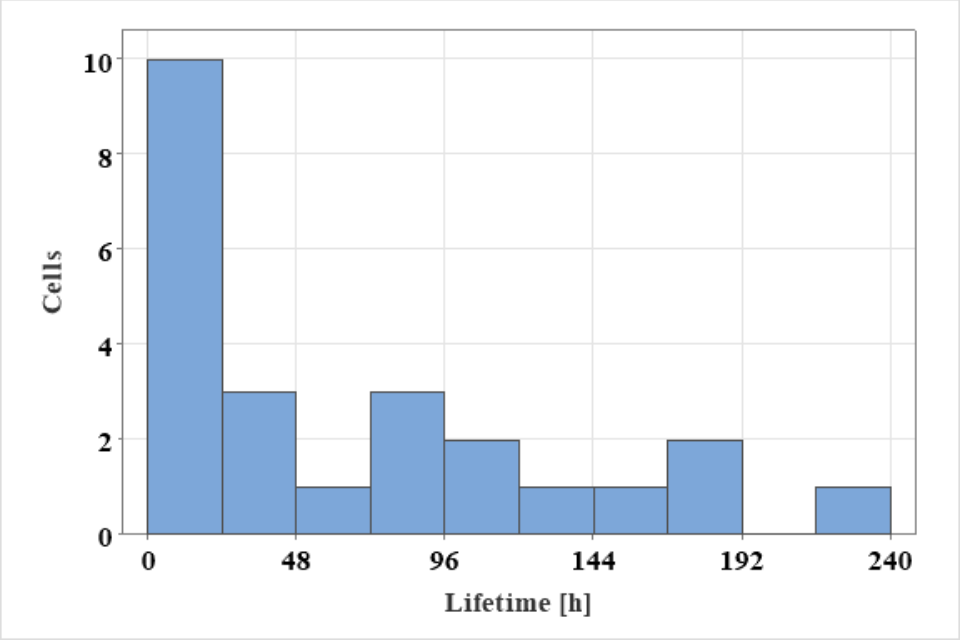


Figure 13. Experiment 1 Cell Lifetime Histogram.

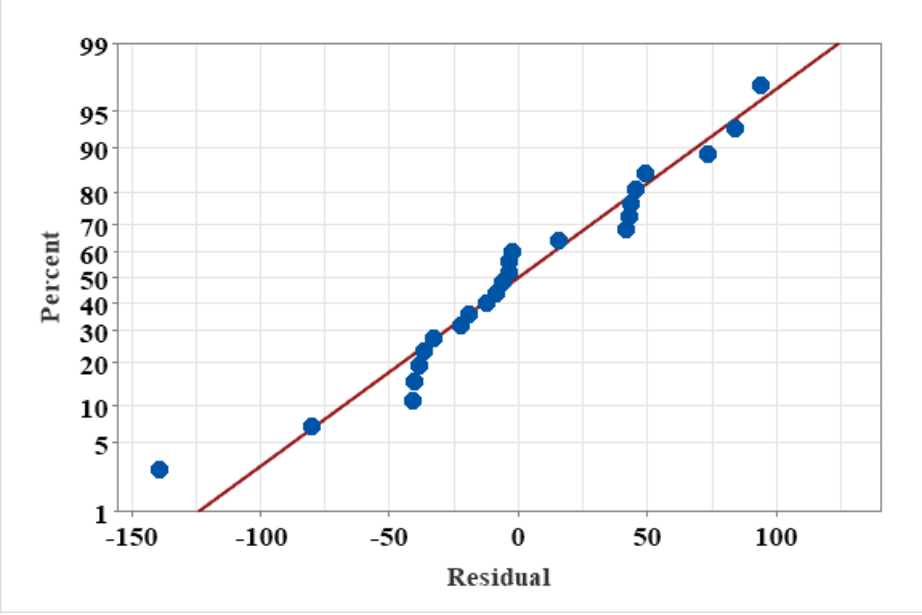


Figure 14. Experiment 1 Cell Lifetime Normal Probability Plot.

For this response, the Pareto chart in Figure 15 shows that the charge/discharge C-rate had a statistically significant effect on the cell lifetime response with a standardized effect of 2.45 versus the critical value of 2.145.

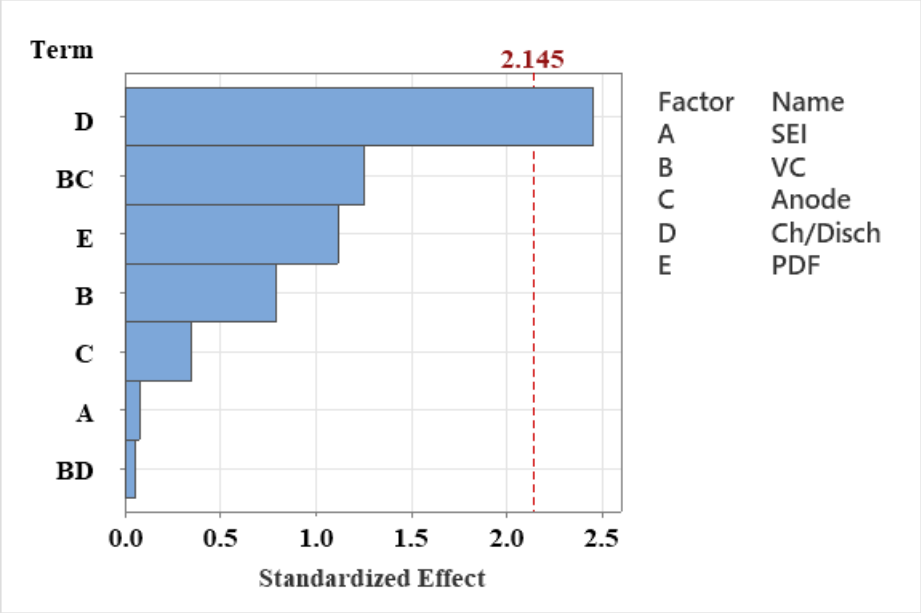


Figure 15. Experiment 1 Cell Lifetime Pareto Chart.

The means plot for the main effect of the charge/discharge c-rate is shown in Figure 16. According to the data, the fitted mean of cell lifetime at 100° C drops from 99.6 hours at C/20 to 30.9 hours at 1C.

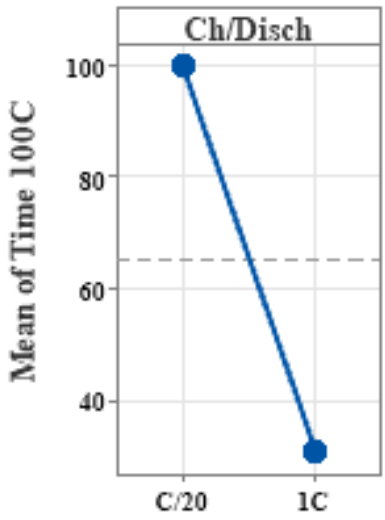


Figure 16. Experiment 1 Cell Lifetime Main Effect Plot.

3.1.2 Discussion

According to the data, the charge/discharge c-rate was the only factor that affected any of the responses. Cells cycled at 1 C averaged 421% as many cycles at 100° C than those cycled at C/20 but spent only 31% as long before cell death at 40% BoL capacity. While it follows logically that a faster charge/discharge rate will cycle more times than a slower one, these results verify that time at 100° C is a cause of battery degradation. Two mechanisms for this degradation are: the instability of electrolytes; and lithium consumption due to increased side reactions at high temperatures for extended periods. The longer the cell spends at 100° C, the worse it performs over time. However, based on previous experiments at JPL with the electrolyte additives, it was expected that the cells would last longer than observed.

It was observed that most of the cells demonstrated discharge capacities within the first five cycles at 100° C of less than 5% their discharge capacity at the end of SEI formation. Some reported coulombic efficiencies higher than 1.1. Considering these to be failed

cells, the failure rate for all the cells in this experiment was 58.3%. This also helps explain the low R^2 values for the models of each response. An additional DOE analysis was performed with a pass/fail response, quantified as pass = 1 and fail = 0. Figure 17 shows that the normal probability plot for pass/fail is not as linear as the other responses, however, is adequate to assume the assumption of normality for this study is valid. The model summary reported an R^2 value of 67.14%.

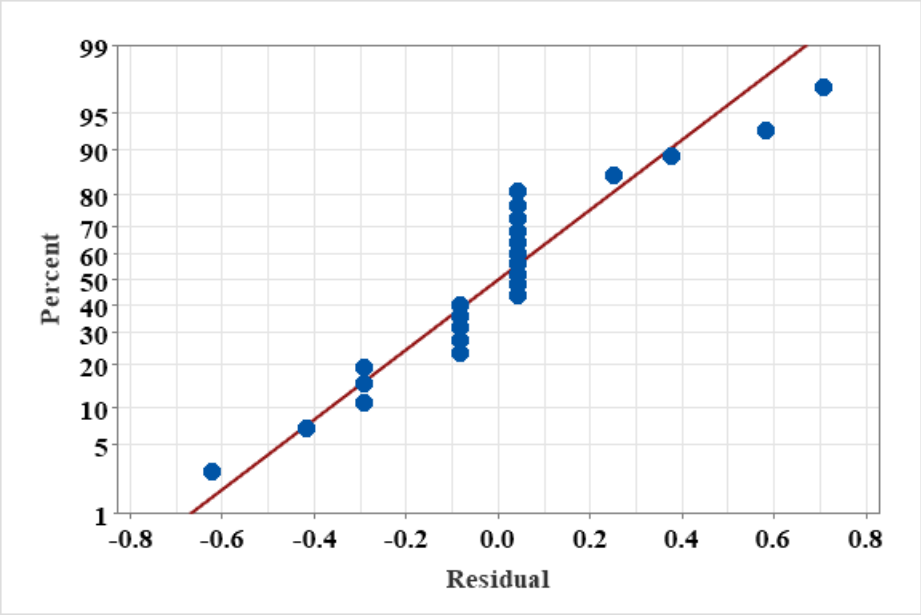


Figure 17. Experiment 1 Pass/Fail Normal Probability Plot.

Analysis found that all factors except the VC additive had a statistically significant main effect on the likelihood of cell failure. Figure 18 shows the Pareto chart of the pass/fail response. In it, the charge/discharge factor dominates the possible causes of failure, but the anode material, SEI formation rate, and PDF additive also contributed to cell failure.

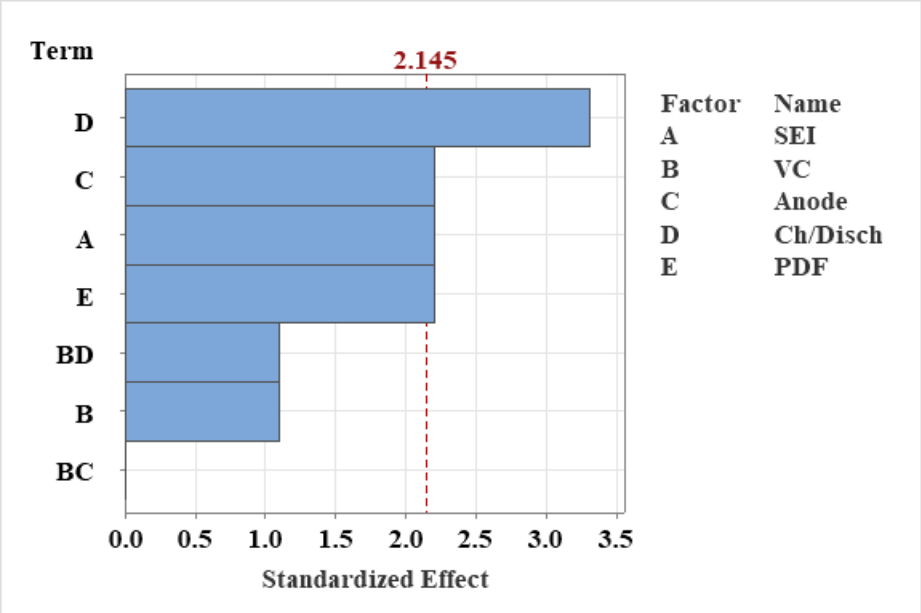


Figure 18. Experiment 1 Pass/Fail Pareto Chart.

In Figure 19, the levels for each factor with a statistically significant effect are shown. It is seen that a slow SEI formation rate, lithium anode, slow charge/discharge rate, and omission of the PDF additive could each be a probable cause of cell failure.

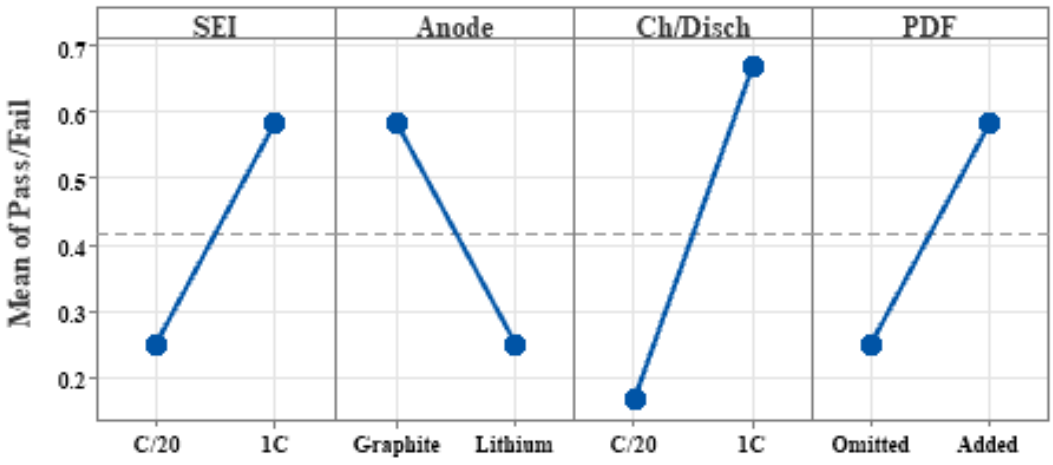


Figure 19. Experiment 1 Pass/Fail Main Effects Plot.

Another reason posited for the high rate of failure was the possibility that an unaccounted-for factor could be contributing to the unreliability of the cells. It was found in literature that the polyethylene layer of Tonen separators has a thermal shutdown temperature of 130° C. With ambient temperatures already at 100° C it was considered that some phenomenon occurring at the separator could be impeding cell operation.

Finally, it was noted that neither the PDF nor VC electrolyte additive showed any significant main effect in the original response data. This was unexpected as previous experiments at JPL had shown otherwise. It was also found that the fractional factorial design used had fully aliased the interaction between PDF and VC, obfuscating any potential interactive effect.

The findings in the fractional factorial experiment led to the decision to design and perform another experiment that would address most of the factors of concern. Results and discussion of the subsequent experiment are detailed in the following section.

3.2 Full Factorial Experiment

In the 2^4 full factorial design, the responses were pass/fail, cycle life, total coulombic efficiency, and end-of-discharge voltage post-rest. In this experiment, the criteria for failure were modified to a demonstration of discharge capacities within the first five cycles at 100° C of less than 5% their discharge capacity at the end of SEI formation or a reported coulombic efficiency higher than 150%. Cycle life was defined as it was in Section 3.1.1. Total coulombic efficiency (Total CE) was defined as the sum of the discharge capacities for each live cycle divided by the sum of the charge capacities for each live cycle as shown in Equation 2,

$$CE = \frac{\sum_{i=1}^{n} discharge\ capacity_i}{\sum_{i=1}^{n} charge\ capacity_i} \quad \text{Eq. 2}$$

where n is the number of live cycles. Lastly, end-of-discharge voltage post-rest (EoD Voltage), which is an indicator of cell impedance, is the recorded cell voltage after the scheduled 15-minute rest period following the discharge cycle.

3.2.1 Experimental Results

Analysis using another developed script for organizing, tabulating, and plotting relevant information was done with MATLAB. Table 5 shows the responses for each of the forty-eight cells. The response data was processed identically to the procedure in Section 3.1.1, except that the pass/fail response was included as part of the analysis as opposed to in addition to, and mean imputation was not necessary as all coulombic efficiency results were valid. Results are presented in the same fashion as the subsections of 3.1.1. Initial analysis did not show a statistically significant fourth-order interaction effect. A second analysis was done, and it was found that all third order interactions included a factor with a much larger main effect on the given response. The Sparsity of Effects principle was not needed to mitigate the effects of aliasing as a full factorial includes all possible trial combinations, however, it was employed to assume that any effects on the responses were caused by the main effect or two-way interactions with statistical significance rather than the third order interactions. As such, the following results sections include plots for analyses considering terms up to second order.

Table 5. Response Values for Full Factorial Experiment.

Cell #	Pass/ Fail	Cycle Life	Total CE	EoD Voltage [V]	Cell #	Pass/ Fail	Cycle Life	Total CE	EoD Voltage [V]
2-1	Pass	50	96%	2.8	2-25	Pass	18	95%	3.2
2-2	Pass	50	95%	2.8	2-26	Pass	16	86%	3.4
2-3	Pass	19	96%	3.2	2-27	Pass	10	42%	2.9
2-4	Pass	35	95%	3.0	2-28	Pass	33	94%	2.9
2-5	Pass	19	61%	3.0	2-29	Pass	14	47%	3.1
2-6	Pass	35	79%	3.1	2-30	Pass	19	90%	3.2
2-7	Pass	27	82%	3.0	2-31	Pass	7	78%	3.2
2-8	Pass	12	59%	3.4	2-32	Pass	13	57%	3.0
2-9	Pass	31	94%	3.1	2-33	Pass	50	95%	2.9
2-10	Pass	19	70%	3.0	2-34	Pass	19	94%	3.0
2-11	Pass	38	97%	2.8	2-35	Pass	50	97%	2.9
2-12	Pass	8	34%	3.1	2-36	Pass	15	38%	3.0
2-13	Pass	36	80%	2.9	2-37	Pass	8	78%	3.1
2-14	Pass	12	65%	3.0	2-38	Pass	21	89%	3.1
2-15	Pass	50	98%	3.0	2-39	Pass	9	28%	3.2
2-16	Pass	17	95%	3.1	2-40	Fail	3	84%	2.7
2-17	Pass	50	93%	2.9	2-41	Pass	50	81%	2.7
2-18	Pass	16	67%	3.0	2-42	Pass	11	48%	3.4
2-19	Pass	20	91%	3.1	2-43	Pass	37	97%	2.9
2-20	Pass	32	88%	3.1	2-44	Pass	26	68%	3.2
2-21	Pass	33	97%	2.9	2-45	Pass	16	75%	3.2
2-22	Pass	50	97%	2.8	2-46	Pass	50	94%	3.1
2-23	Pass	23	78%	3.1	2-47	Pass	31	95%	2.8
2-24	Pass	50	97%	2.8	2-48	Pass	8	72%	3.4

3.2.2.1 Pass/Fail

In this experiment, only one cell met the criteria for a “fail” response. Cell 2-40 completed three complete cycles, then appears to have experienced a persistent discharge in the fourth cycle as shown in Figure 20. As mentioned in Section 2.3, since the cell failed to meet the target discharge voltage of 2500mV within 48 hours, the test ended. Since all five initial cycles at 100° C did not exceed 5% of the final discharge capacity after the SEI formation stage, the cell registered a “fail” response.

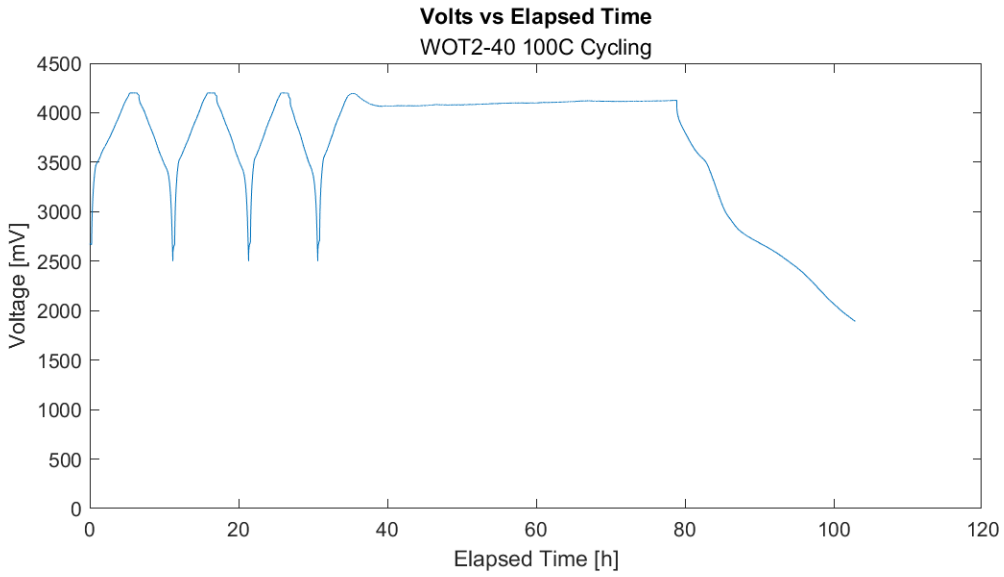


Figure 20. Cell 2-40 Voltage vs Elapsed Time.

Consequently, with only one failed cell out of the trial sample, there is almost no variability in the data. The normal probability plot in Figure 21 shows the residuals for pass/fail falling in a series of straight lines and for cell 2-40 on the extreme bottom left. Since this plot would not pass the "fat pencil test," the assumption of normally distributed data cannot be validated and thus the parametric statistical tests performed by Minitab would not be appropriate for drawing statistical inference. The model summary reported an R^2 value of 34.04%.

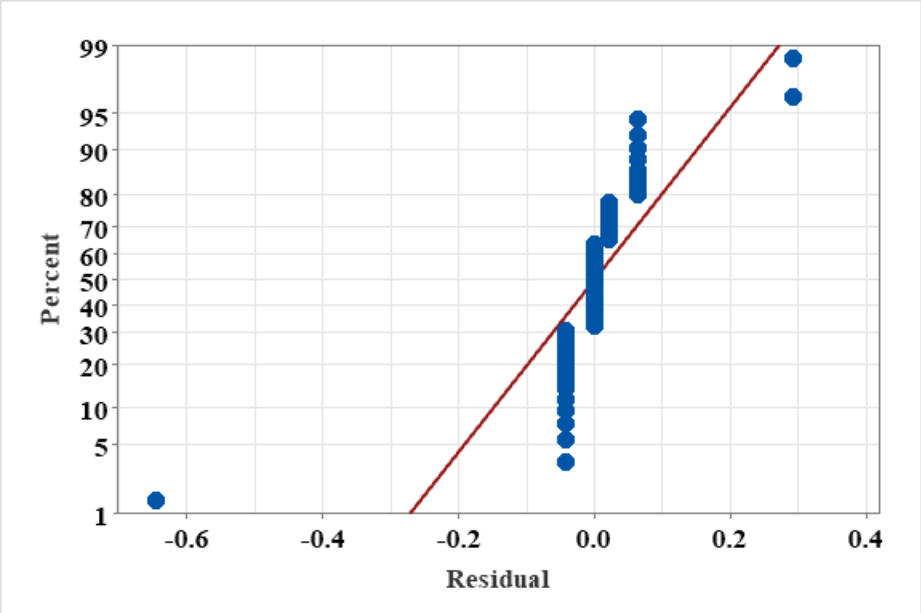


Figure 21. Experiment 2 Pass/Fail Normal Probability Plot.

3.2.2.2 Cycle Life

In Figure 22, the normal probability plot for Cycle Life shows that the assumption of normally distributed data can be considered valid. Although the residual point for WOT2-26 is noticeably far to the left of the line of reference, it may be within the limit for an assumption of normality. Additionally, with only one residual in question out of forty-eight, it is appropriate to proceed with analysis [25]. The model summary reported an R^2 value of 76.17%.

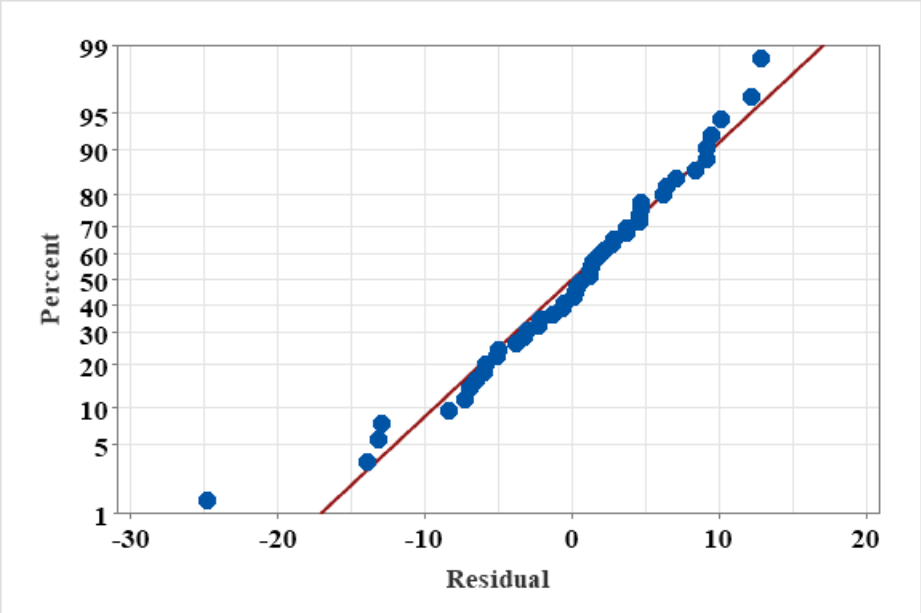


Figure 22. Experiment 2 Cycle Life Normal Probability Plot.

Figure 23 shows the Pareto chart for Cycle Life with a critical value of 2.03. The model terms with a statistically significant effect on the number of live cycles recorded and their standardized effect were Separator at 7.95, Cathode*Separator at 4.13, Cathode at 3.52, PDF*Separator at 2.47, and PDF*Cathode at 2.10. The null hypothesis must be rejected for each of these model terms as the corresponding P-values are each under the α-level of 0.05.

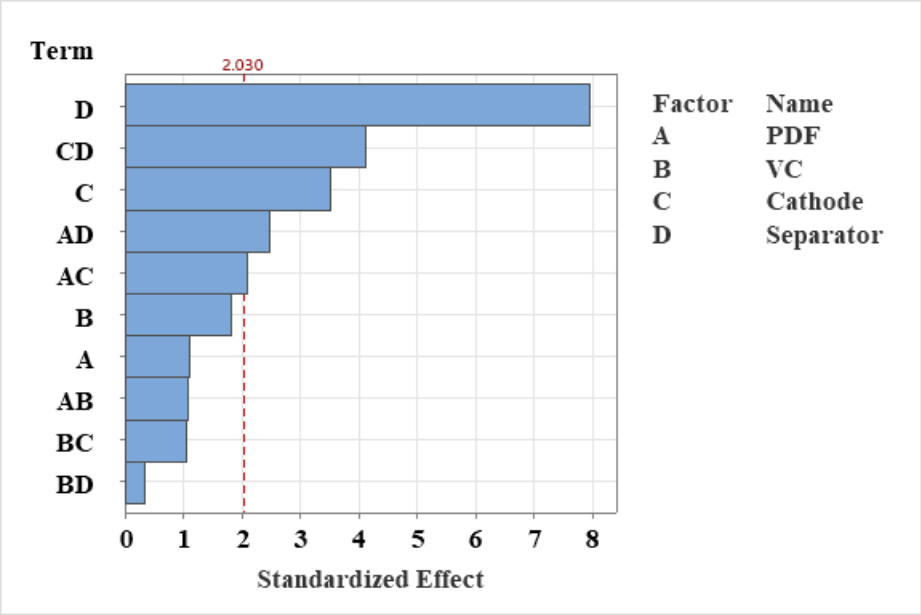


Figure 23. Experiment 2 Cycle Life Pareto Chart.

In cells made with a Polyimide separator, the fitted mean showed a 118.2% increase compared to Tonen, from 16.58 cycles to 36.17 cycles. In cells made with 8:1:1 cathode, mean showed a 28.2% decrease compared to 1:1:1, from 30.71 cycles to 22.04 cycles. The means plot for main effects in Figure 24 illustrates the change in the fitted mean for Cycle Life between levels of each factor.

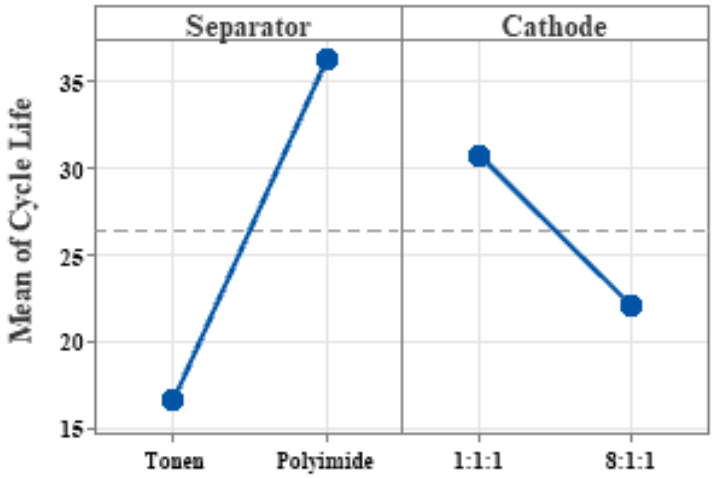


Figure 24. Experiment 2 Cycle Life Main Effects Plot.

In cells made with Tonen separator, and with 8:1:1 cathode, the mean showed a 9.5% increase compared to 1:1:1, from 15.83 cycles to 17.33 cycles. In cells made with Polyimide separator, and with 8:1:1 cathode, the mean showed a 41.3% decrease compared to 1:1:1, from 45.58 cycles to 26.75 cycles.

In cells made with Tonen separator, and with PDF added, the fitted mean showed a 72.6% increase compared to PDF omitted, from 12.17 cycles to 21 cycles. In cells made with Polyimide separator, and with PDF added, mean showed an 8.8% decrease compared to PDF omitted. From 37.83 cycles to 34.5 cycles.

In cells made with 1:1:1 cathode, and with PDF added, mean showed a 29.6% increase compared to PDF omitted, from 26.75 cycles to 34.67 cycles. In cells made with 8:1:1 cathode, and with PDF added, mean showed a 10.4% decrease compared to PDF omitted, from 23.25 cycles to 28.3 cycles. The means plot for factor interactions with statistically significant effects is shown here in Figure 25.

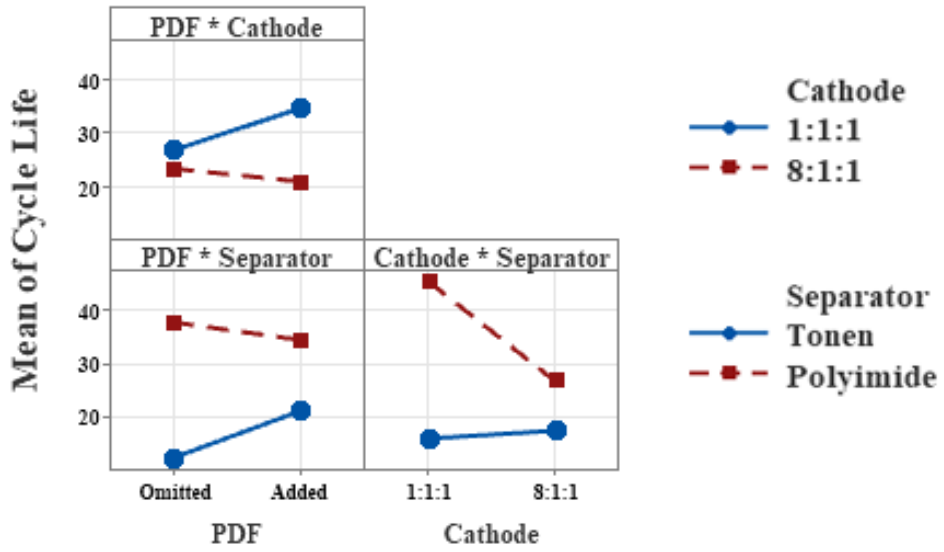


Figure 25. Experiment 2 Cycle Life Interactive Effects Plot.

3.2.2.3 Total Coulombic Efficiency

The Normal Probability Plot for Total CE is shown in Figure 26, all residual data falls sufficiently close to reference line validating the assumption of normal distribution. The model summary reported an R^2 value of 69.01%.

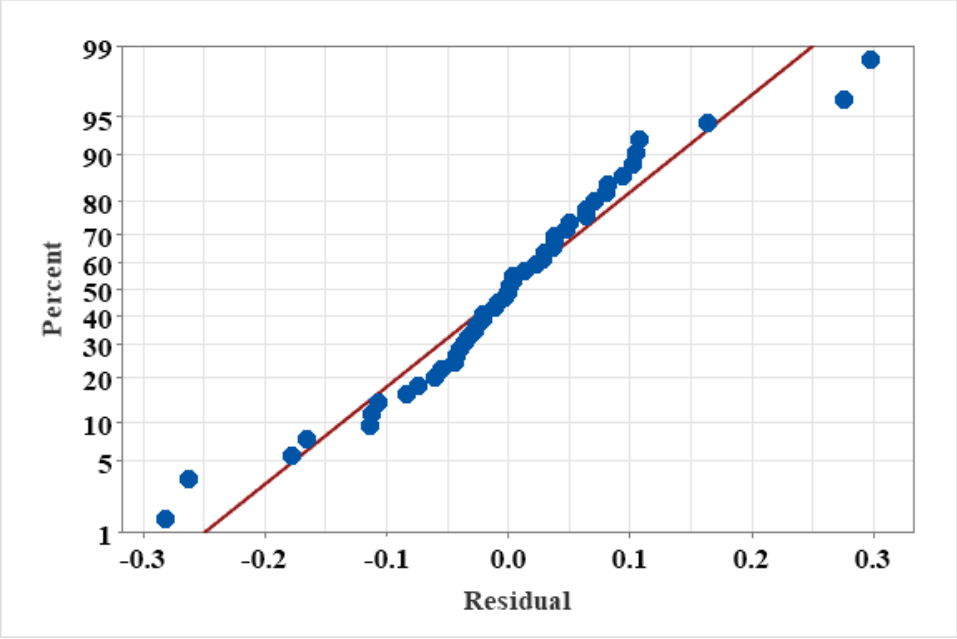


Figure 26. Experiment 2 Total Coulombic Efficiency Normal Probability Plot.

The Pareto chart for Total CE is shown in Figure 27 with a critical value of 2.030. The only model term with a statistically significant effect on the response is the Separator with a standardized effect value of 8.00.

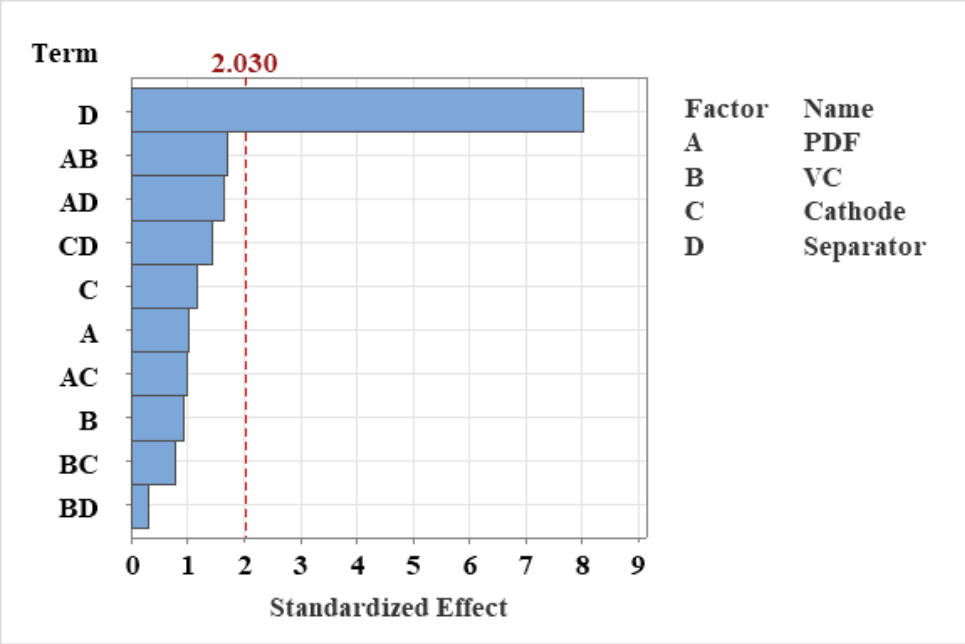


Figure 27. Experiment 2 Total Coulombic Efficiency Pareto Chart.

Figure 28 shows the positive effect of the Polyimide separator on the fitted mean of Total CE. In cells made with a Polyimide separator, the mean showed a 44.2% increase compared to Tonen, From 65.29% to 94.14%.

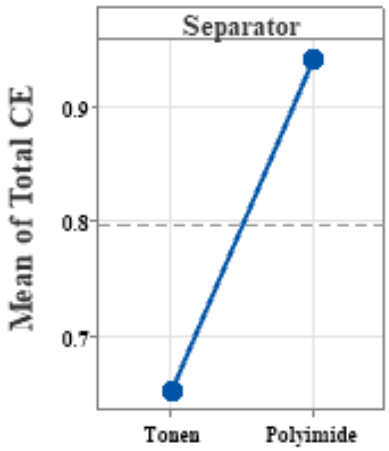


Figure 28. Experiment 2 Total Coulombic Efficiency Main Effect Plot.

3.2.2.4 End-of-Discharge Voltage Post-Rest

The Normal Probability plot is shown here in Figure 29. As with the other responses, the residuals are sufficiently close to the line of normal distribution for the linear model for the use of parametric tests.

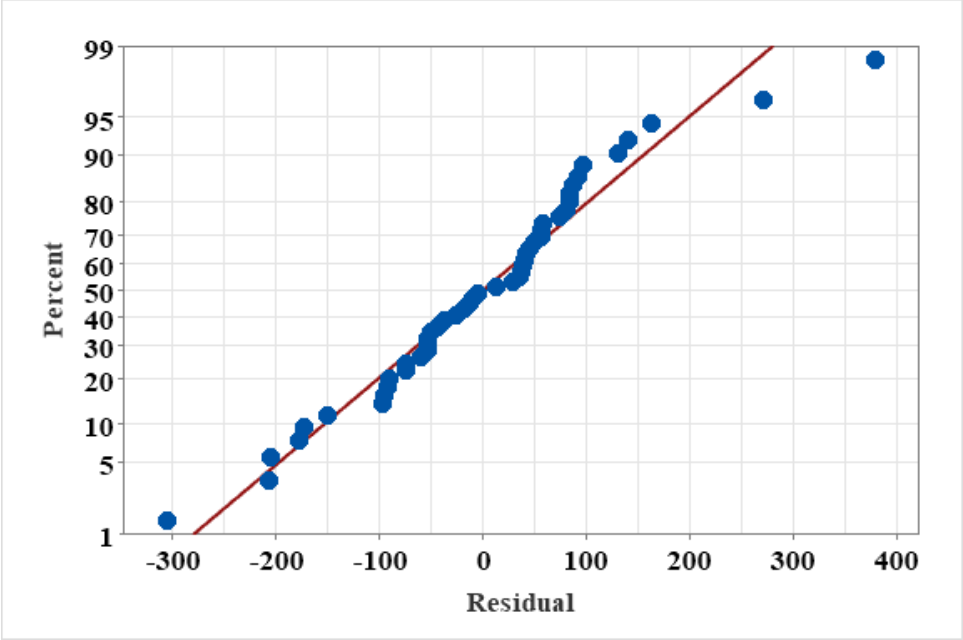


Figure 29. Experiment 2 End-of-Discharge Voltage Post-Rest Normal Probability Plot.

The Pareto chart for EoD Voltage is found in Figure 30, again with a critical value of 2.030. This chart shows statistically significant standardized effects from the model terms PDF*Cathode at 4.48, Separator at 3.68, and Cathode*Separator at 2.97.

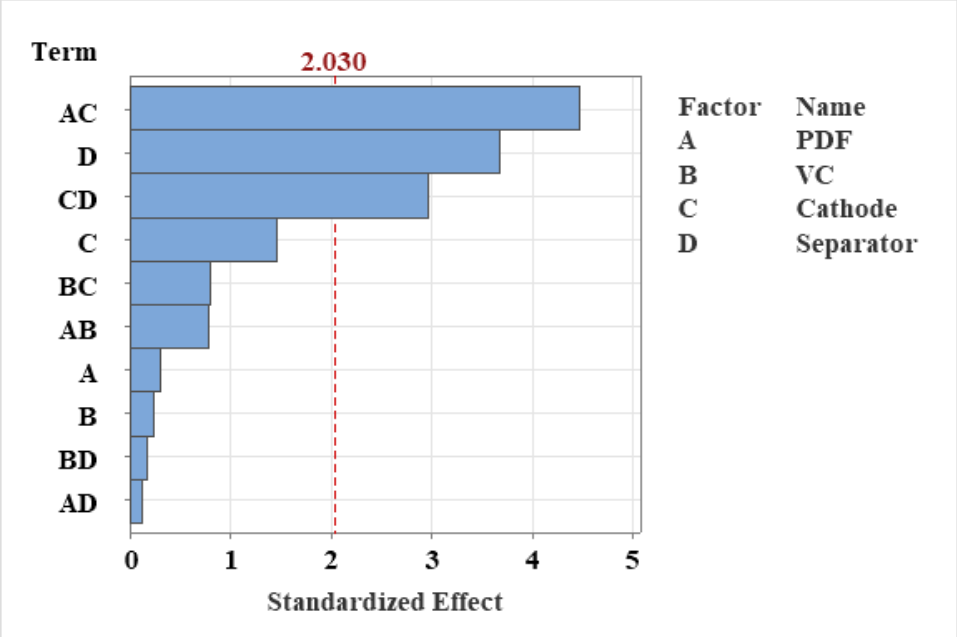


Figure 30. Experiment 2 End-of-Discharge Voltage Post-Rest Pareto Chart.

Figure 31 shows the main effect on the fitted means for EoD Voltage. In cells made with Polyimide, the fitted mean showed a 4.8% decrease compared to Tonen, from 3101.2 mV to 2952.9 mV.

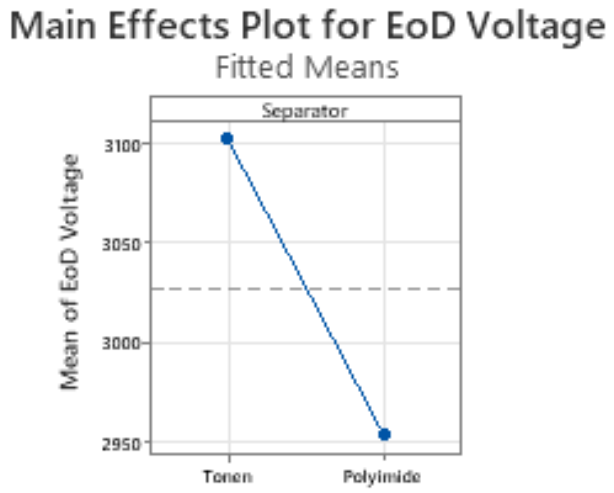


Figure 31. Experiment 2 End-of-Discharge Voltage Post-Rest Main Effect Plot.

The interaction plot for fitted means is shown in Figure 32. In cells made with 1:1:1 cathode, and with PDF added, the EoD Voltage mean showed a 5.4% decrease compared to omitted, from 3140.6 mV to 2972.5 mV. In cells made with 8:1:1 cathode, and with PDF added, the mean showed a 6.7% increase compared to omitted, from 2901.0 mV to 3094.2 mV.

In cells made with a Tonen separator, and with an 8:1:1 cathode, the fitted mean showed a 5.6% decrease compared to 1:1:1, from 3190.6 mV to 3011.9 mV. While cells made with Polyimide separator, and with 8:1:1 cathode, mean showed a 2.1% increase compared to 1:1:1, from 2922.6 mV to 2983.3 mV.

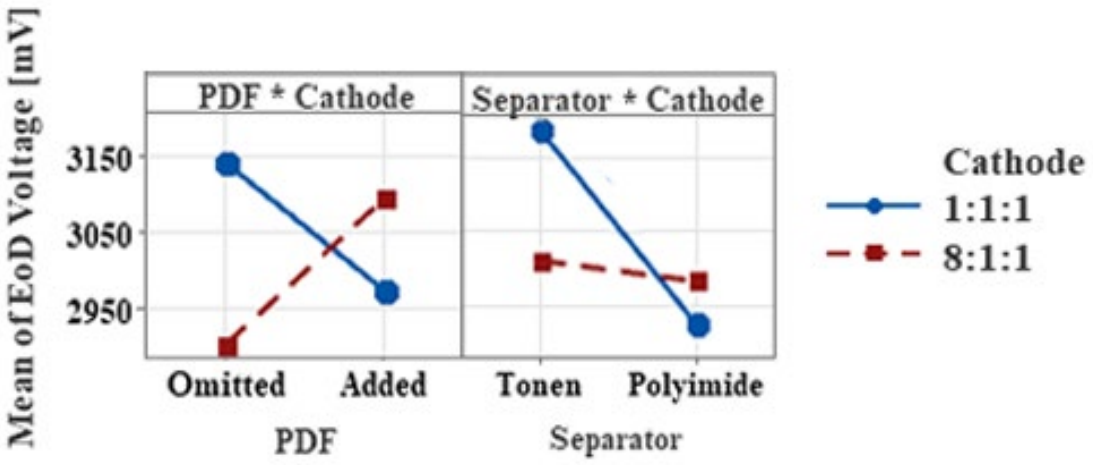


Figure 32. Experiment 2 End-of-Discharge Voltage Post-Rest Interactive Effects Plot.

3.2.2 Discussion

The second experiment in this study was vastly successful compared to the first in that only one cell failed, according to the established criteria of the first response. This allowed for a robust analysis of the other responses, where even the failed cell had contributable data. While the Pass/Fail response was not able to undergo statistical analysis due to a lack of response variability, the raw experimental results confirm that the factor levels associated with failure in the preliminary experiment could be screened out of subsequent experiments, leading to more useful results. The following discussion will focus on the factor levels in this experiment that had the greatest overall impact on the response variables and will address the absence of certain expected results.

The polyimide separator proved to be the most consequential factor level in this study, displaying statistically significant main effects on cycle life, total CE, and EoD voltage. While the operating temperature of the specific polyimide used was not disclosed, Kapton, a commercially successful polyimide film product made by Dupont, is

thermally stable up to 400° C [26]. The Tonen tri-layer separator, however, has a polyethylene layer designed to prevent thermal runaway by melting at 130° C, thus blocking the separator pores and blocking the transport of lithium ions between electrodes. It is possible that, although the cells are cycled in a thermal chamber set to 100° C, the chemical reactions occurring inside the cell may increase the internal temperature, causing the thermal shutoff designed into Tonen separators. Stemming from these findings, tests at JPL have discovered previously unknown chemical reactions taking place in the Tonen separators. This difference in thermal stability could be a reason for the improved performance in all three metrics as the Polyimide separator would continue to allow the unimpeded transport of lithium ions through it. Cells with a Tonen separator in the process of thermal shutdown would see an increase in resistance, increasing EoD Voltage. This increased resistance could be forcing lithium ions into sites where they would no longer be available for charge transfer, resulting in a loss of active material which would lead to decreased cycle life and coulombic efficiency.

Polyimide was also involved in two statistically significant antagonistic interactions affecting cycle life and one antagonistic interaction affecting EoD Voltage. However, in all three cases, even though the Polyimide cells saw a negative effect on the response compared to Tonen when paired with the same factor, the response mean was still favorable to polyimide, e.g., in cycle life, the use of polyimide with added PDF produced an 8.8% decrease as compared to when PDF was omitted, whereas cycle life improved by 72.6% in cells that used Tonen when PDF was added. However, the decreased response with polyimide was still higher than the improved response with Tonen (34.5 to 21 cycles).

The next biggest improvement in performance came from the main effect of the 1:1:1 NMC cathode. Cycle life was improved by 39.3% when the 1:1:1 cathode was used versus the 8:1:1 NMC cathode. The latter was originally proposed as an alternative because other studies at JPL have shown a higher energy density than the former, however, for the tested responses at 100° C, this characteristic did not improve the response means. Additionally, it has been found that high-nickel ternary cathode materials can display structural instability and decreased cycling stability [27].

The 1:1:1 cathode was also involved in statistically significant interactions; with the separator and with the PDF in cycle life, and again with those two factors in EoD voltage. In cycle life, the synergistic interaction with polyimide showed that, while the more robust separator added almost 9.5 cycles to cells with an 8:1:1 cathode, with the 1:1:1 cathode, almost 30 cycles were added. With the 8:1:1 cathode, adding PDF resulted in 2.42 less cycles, however, adding PDF in a cell with a 1:1:1 cathode caused an increase of 7.92 cycles. Again, these results could stem from the possible increase in heat generation with the 8:1:1 cathode.

Lastly, there was something noticeably missing from all the resultant data. One of the original goals of introducing DOE methodology in li-ion cell testing at JPL was to explore the possible interactive effects between the electrolyte additives that were factors in both experiments in this study. Previous studies had shown improvement in cell performance attributed to both PDF and VC. However, only PDF was present in any statistically significant effects and only when interacting with the separator or the cathode, which, as previously discussed, are more likely to be responsible for an effect on the response. The idea was proposed that, the ratio of volume of electrolyte solution to

active material used in these experiments was exceptionally large compared to commercial batteries or other batteries tested at JPL and could be obfuscating any positive effects caused by the electrolyte additives.

CHAPTER 4

Conclusions

4.1 Summary

The full factorial experiment was successful in determining the dominance of the Polyimide separator material in improving cell performance and the superiority of the 1:1:1 NMC cathode at 100° C. Having data for every trial combination left little room for ambiguity in the response results. The fractional factorial design was useful in determining a more optimized experimental design. It also highlighted the importance of thinking critically about the effects of not only the factors being tested, but also those not being tested. Without the high failure rate seen in the first experiment, the importance of the separator material would not have been discovered. This discovery led JPL to perform an Attenuated Total Reflectance (ATR) Spectroscopy analysis of the Tonen separator, which found changes to the polyolefin surface below the thermal shutdown temperature of the polyethylene layer.

Another such factor was not tested but may have affected the responses was the volume of electrolyte solution used. For both experiments, 100µL of solution was dropped into each cell. The lack of any statistically significant main effect by either electrolyte additive or interaction between the two on any of the responses, was unexpected. The uncommonly high electrolyte volume to active material ratio may limit the positive effects of the additives seen in previous experiments.

4.2 Conclusion

Design of Experiments is a powerful tool for characterizing the effects of multiple factors on experimental responses. The purpose of this research was to evaluate the

viability of utilizing full and fractional factorial DOE to optimize the performance of lithium-ion coin cells at a high operating temperature in support of the Venus Aerobot mission at JPL.

In this study, two experiments, one full and one fractional 2^k factorial design, were designed and conducted to quantitatively analyze and compare the main and interactive effects of a total of seven lithium-ion coin cell components on a total of six responses. Completion of the study required experiment design, cell assembly, solid electrolyte interphase formation, high-temperature cycling, experimental data analysis, and statistical analysis.

The results of the fractional factorial design verified, among other factors, the instability of a lithium anode at 100°C. The full factorial design showed the polyimide separator had the most significant positive effect on cycle life – improving it by 118.2% over the tri-layer Tonen, the most significant positive effect on total coulombic efficiency – showing a 44.2% improvement over Tonen, and the second highest positive effect on end-of-discharge voltage post-rest with a drop of 4.8%. Additionally, the 1:1:1 NMC cathode proved to be the superior cathode material, showing a 39.3% improvement to cycle life over the 8:1:1.

A more rigorous approach to planning fractional factorial DOEs is suggested as the aliasing effect inherent in the fractional design can make it difficult to glean useful information, especially when interactive effects are the research focus. A Resolution IV design may serve its intended purpose of saving time and resources if special attention is paid to the alias structure during the initial design stage. Nevertheless, factorial DOE

methodologies have, in this study, proven useful in the development of high-temperature lithium-ion batteries.

4.2 Future Work

In partnership with JPL, further experiments are planned to continue the work presented in this study. A one-variable-at-a-time (OVAT) experiment will use the factors that led to the best cell performance found in this work to test the effect of electrolyte volume. Once a favorable range is discovered, further DOE designs will be used to continue the optimization of mission-enabling lithium-ion batteries.

REFERENCES

[1] J. Tieu, *Project Titlle: 14200 Development of Wide Operating Temperature Batteries Via Design-of-Experiment (DOE) Studies of Electrolyte Formulations,* Pasadena, CA: Jet Propulsion Laboratory, 2023.

[2] The Roadmap Development Team, "Mission to the Solar System: Exploration and Discovery A Mission and Technology Roadmap," Jet Propulsion Laboratory, Pasadena, 1998.

[3] J. G. O'Rourke, C. F. Wilson, M. E. Borrelli and e. al, "Venus, the Planet: Introduction to the Evolution of Earth's Sister Planet," *Space Science Reviews,* vol. 219, no. 10 (2023), p. 10, 06 February 2023.

[4] J. L. Hall, J. S. Izraelevitz, J. A. Cutts, K. H. Baines and P. Byrne, "Venus Aerobot Science and Operations Concepts," in *COSPAR 2021*, Sydney, Australia, 2021.

[5] J. L. Hall, J. S. Izraelevitz, M. T. Pauken, J. M. Cameron, H. Patel, T. Lachenmeier, T. Elder and C. Turner, "Venus Aerobot Prototype Development," in *COSPAR 2021*, Sydney, Australia, 2021.

[6] D. Deng, "Li-ion batteries: basics, progress, and challenges," *Energy Science and Engineering,* vol. 3, no. 5, pp. 385-418, 2015.

[7] Epec Engineered Technologies, "Battery Cell Comparison," 2024. [Online]. Available: https://www.epectec.com/batteries/cell-comparison.html.

[8] J. C. Bachman, "Organic Electrodes and Solid-State Electrolytes for Lithium Electrochemical Energy Storage," Massachusetts Institute of Technology, Massachusetts, 2017.

[9] F. Wu, F. Chu and Z. Xue, "Lithium-Ion Batteries," in *Encyclopedia of Energy Storage*, vol. 4, L. F. Cabeza, Ed., Elsevier, 2022, pp. 5-13.

[10] S. Ma, M. . Jiang, P. Tao, C. Song, J. . Wu, J. Wang, T. . Deng and W. Shang, "Temperature effect and thermal impact on lithium-ion batteries: A review," *Progress in Natural Science: Materials International,* vol. 28, no. 6, pp. 653-666, Dec 2018.

[11] M. Ghiji, V. Novozhilov, K. Moinuddin and P. . Joseph, "A Review of Lithium-Ion Battery Fire Suppresion," *Energies,* vol. 13, 2020.

[12] A. Pesaran, S. Santhanagopalan and G.-H. Kim, "Addressing the Impact of Temperature Extremes on Large Format Li-Ion Batteries for Vehicle Applications," in *30th International Battery Seminar*, Ft. Lauderdale, FL, 2013.

[13] M. Alipour, C. Ziebert, F. V. Conte and R. Kizilel, "A Review on Temperature-Dependent Electrochemical Properties, Agin, and Performance of Lithium-Ion Cells," *Batteries,* vol. 6, no. 3:35, 2020.

[14] J. S. Edge, S. O'Kane, R. Prosser, N. Kirkaldy, A. N. Patel, A. Hales, A. Ghosh, W. Ai, J. Chen, J. Yang, S. Li, M.-C. Pang, L. B. Diaz , A. Tomaszewka, M. W. Marzook, K. N. Radhakrishnan, H. Wang, Y. . Patel, B. Wu and G. J. Offer, "Lithium ion battery degradation: what you need to know," *Phys. Chem. Chem. Phys.,* vol. 23, pp. 8200-8221, 2021.

[15] F. T. Geldasa, M. A. Kebede, M. W. Shura and F. G. Hone, "Identifying surface degradation, mechanical failure,and thermal instability phenomena of high energy density Ni-rich NCM cathode materials for lithium ion batteries: a review," *RSC Advances,* vol. 12, pp. 5891-5909, 2022.

[16] G. Ning, B. Haran and B. N. Popov, "Capacity fade study of lithium-ion batteries cycled at high discharge rates," *Journal of Power Sources,* vol. 17, no. 1-2, pp. 160-169, 2003.

[17] F. Leng, C. M. Tan and M. Pecht, "Effect of Temperature on the Aging rate of Li Ion Battery Operating above Room Temperature," *Nature,* vol. 5, pp. 1-12, 6 August 2015.

[18] L. Román-Ramírez and J. Marco, "Design of experiments applied to lithium-ion batteries: A literature review," *Applied Energy,* vol. 320, 2022.

[19] J. Antony, Design of Experiments for Engineers and Scientists, Oxford: Butterworth-Heinemann, 2003.

[20] D. C. Montgomery and G. C. Runger, Applied Statistics and Probability for Engineers, 6th Edition, Hoboken: Wiley, 2013.

[21] A. J. Wheeler and A. R. Ganji, Introduction to Engineering Experimentation, 3rd Edition, Boston: Prentice Hall, 2010.

[22] D. C. Montgomery, Design and Analysis of Experiments, Hoboken: John Wiley & Sons, Inc., 2013.

[23] E. Raheem, "Missing Data Imputation," in *Statistical Approaches for Epidemiology*, Springer, Cham, 2023, pp. 293-316.

[24] M. Support, "Normal probability plots and the "fat pencil test"," Minitab, 2024. [Online]. Available: https://support.minitab.com/en-us/minitab/help-and-how-to/statistics/basic-statistics/supporting-topics/normality/normal-probability-plots-and-the-fat-pencil-test/.

[25] M. Support, "What to do with nonnormal data," Minitab, 2024. [Online]. Available: https://support.minitab.com/en-us/minitab/help-and-how-to/statistics/basic-statistics/supporting-topics/normality/what-to-do-with-nonnormal-data/.

[26] Dupont, "DuPont Kapton Summary of Properties," 2022. [Online]. Available: https://www.dupont.com/content/dam/dupont/amer/us/en/ei-transformation/public/documents/en/EI-10142_Kapton-Summary-of-Properties.pdf.

[27] Y. Li, Z. Tan, Y. Liu, C. Lei, P. He, J. Li, Z. He, Y. Cheng, F. Wu and Y. Li, "Past, present and future of high-nickel materials," *Nano Energy,* 2024.

[28] Z. Lu, F. Sui, Y.-E. . Maio, G. Liu, C. Li, W. Dong, J. Cui, T. Liu, J. Wu and C. Yang, "Polyimide separators for rechargeable batteries," *Journal of Energy Chemistry,* vol. 58, pp. 170-197, 2021.

APPENDIX

Experimental Layouts

Table A - 1. Experimental Layout for Fractional Factorial Design.

Std	Run	Blocks	SEI	Ch/Disch	PDF	Anode	VC
2	17	1	1C	C/20	Added	Lithium	Added
4	18	1	1C	1C	Added	Graphite	Added
3	19	1	C/20	1C	Added	Lithium	Omitted
7	20	1	C/20	1C	Omitted	Lithium	Added
8	21	1	1C	1C	Omitted	Graphite	Omitted
5	22	1	C/20	C/20	Omitted	Graphite	Added
6	23	1	1C	C/20	Omitted	Lithium	Omitted
1	24	1	C/20	C/20	Added	Graphite	Omitted
12	1	2	1C	1C	Added	Graphite	Added
15	2	2	C/20	1C	Omitted	Lithium	Added
10	3	2	1C	C/20	Added	Lithium	Added
14	4	2	1C	C/20	Omitted	Lithium	Omitted
16	5	2	1C	1C	Omitted	Graphite	Omitted
13	6	2	C/20	C/20	Omitted	Graphite	Added
9	7	2	C/20	C/20	Added	Graphite	Omitted
11	8	2	C/20	1C	Added	Lithium	Omitted
24	9	3	1C	1C	Omitted	Graphite	Omitted
19	10	3	C/20	1C	Added	Lithium	Omitted
22	11	3	1C	C/20	Omitted	Lithium	Omitted
17	12	3	C/20	C/20	Added	Graphite	Omitted
18	13	3	1C	C/20	Added	Lithium	Added
21	14	3	C/20	C/20	Omitted	Graphite	Added
23	15	3	C/20	1C	Omitted	Lithium	Added
20	16	3	1C	1C	Added	Graphite	Added

Table A - 2. Experimental Layout for Fractional Factorial Design.

Std Order	Run Order	Blocks	PDF	VC	Cathode	Separator
44	1	3	Added	Added	1:1:1	Polyimide
42	2	3	Added	Omitted	1:1:1	Polyimide
48	3	3	Added	Added	8:1:1	Polyimide
45	4	3	Omitted	Omitted	8:1:1	Polyimide
38	5	3	Added	Omitted	8:1:1	Tonen
34	6	3	Added	Omitted	1:1:1	Tonen
36	7	3	Added	Added	1:1:1	Tonen
33	8	3	Omitted	Omitted	1:1:1	Tonen
41	9	3	Omitted	Omitted	1:1:1	Polyimide
39	10	3	Omitted	Added	8:1:1	Tonen
47	11	3	Omitted	Added	8:1:1	Polyimide
35	12	3	Omitted	Added	1:1:1	Tonen
40	13	3	Added	Added	8:1:1	Tonen
37	14	3	Omitted	Omitted	8:1:1	Tonen
43	15	3	Omitted	Added	1:1:1	Polyimide
46	16	3	Added	Omitted	8:1:1	Polyimide
12	17	1	Added	Added	1:1:1	Polyimide
1	18	1	Omitted	Omitted	1:1:1	Tonen
14	19	1	Added	Omitted	8:1:1	Polyimide
8	20	1	Added	Added	8:1:1	Tonen
13	21	1	Omitted	Omitted	8:1:1	Polyimide
11	22	1	Omitted	Added	1:1:1	Polyimide
2	23	1	Added	Omitted	1:1:1	Tonen
10	24	1	Added	Omitted	1:1:1	Polyimide
16	25	1	Added	Added	8:1:1	Polyimide
9	26	1	Omitted	Omitted	1:1:1	Polyimide
5	27	1	Omitted	Omitted	8:1:1	Tonen
15	28	1	Omitted	Added	8:1:1	Polyimide
6	29	1	Added	Omitted	8:1:1	Tonen
3	30	1	Omitted	Added	1:1:1	Tonen
4	31	1	Added	Added	1:1:1	Tonen
7	32	1	Omitted	Added	8:1:1	Tonen
25	33	2	Omitted	Omitted	1:1:1	Polyimide
30	34	2	Added	Omitted	8:1:1	Polyimide
27	35	2	Omitted	Added	1:1:1	Polyimide
23	36	2	Omitted	Added	8:1:1	Tonen
20	37	2	Added	Added	1:1:1	Tonen
32	38	2	Added	Added	8:1:1	Polyimide
22	39	2	Added	Omitted	8:1:1	Tonen

Std Order	Run Order	Blocks	PDF	VC	Cathode	Separator
21	40	2	Omitted	Omitted	8:1:1	Tonen
26	41	2	Added	Omitted	1:1:1	Polyimide
19	42	2	Omitted	Added	1:1:1	Tonen
31	43	2	Omitted	Added	8:1:1	Polyimide
24	44	2	Added	Added	8:1:1	Tonen
18	45	2	Added	Omitted	1:1:1	Tonen
28	46	2	Added	Added	1:1:1	Polyimide
29	47	2	Omitted	Omitted	8:1:1	Polyimide
17	48	2	Omitted	Omitted	1:1:1	Tonen